Velocity skew controls the flushing of a tracer in a system of shallow bays with multiple inlets

I. Palazzoli[1,2], N. Leonardi[3], A. M. Jiménez-Robles[1,4], S. Fagherazzi[1]

[1]Department of Earth and Environment, Boston University, Boston, MA, USA.

[2]Department of Civil, Chemical, Environmental and Materials Engineering, University of Bologna, Italy.

[3]Department of Geography and Planning, University of Liverpool, Liverpool, UK.

[4]Environmental Fluid Dynamics Group, Andalusian Institute for Earth System Research, University of Granada, Granada, Spain.

Corresponding author: Irene Palazzoli (irene.palazzoli@unibo.it)

Key Points:

- Wind currents and differences in tidal phase and amplitude along the inner shelf are an effective mechanism for flushing tracer out of a coastal bay with multiple inlets
- Velocity skew at the inlets directly controls the tracer flushing time
- A simple, single-parameter exponential model is used to determine the decrease in tracer mass in the coastal bays

Abstract

The exchange of dissolved constituents between a shallow bay and the ocean is governed by regular tidal fluxes as well as by wind generated storm surges and currents. These mechanisms regulate the rate at which pollutants and nutrients are removed from the lagoons. Here we determine the main hydrodynamic drivers controlling the removal of a conservative tracer from a bay with multiple inlets. The transport of the tracer is simulated using the numerical model Delft3D in a system of shallow lagoons along the coast of the Delmarva Peninsula, Virginia. The tracer flushing time is evaluated using the Eulerian approach and the decay of the tracer concentration in time is approximated with an exponential curve. We assess the influence of tidal amplitude, local winds, and time of release of the tracer with respect to the tidal cycle on flushing time. Results show that wind-driven fluxes are a prevailing factor controlling the tracer transport and, therefore, the tracer concentration within the lagoons. Variations in tidal phase and amplitude along the inner shelf also promote the flushing of the tracer out of the bays, while the time of tracer release with respect to the tidal phase has been found to play a relatively negligible role. The tracer flushing time is proportional to a velocity skew index, accounting for the asymmetry of the ebb-flood velocities at the inlets, while the tidal prism has minimal effect on flushing time. Our simulations revealed that the average flushing time of these bays is around 24-27 days, decreasing to 21 days if favorable wind conditions exist. Finally, a simplified approach is presented to compute the decay of tracer concentration in time as a function of hourly variable wind characteristics as well as seasonal changes in meteorological conditions, without the need of large scale simulations.

1 Introduction

Estuaries and bays are affected by the release of pollutants and nutrients that deteriorate water quality and put ecosystems at risk (e.g. Cavalcante et al. [2012]). Therefore, there is a need to determine the fate of these pollutants and quantify how long it takes for the pollutant to be exported to the open ocean. The decay rate and the flushing time of contaminants injected into a bay is regulated by coastal hydrodynamics [Braunschweig et al., 2003].

Fugate et al. [2006] estimated the spatial distribution of residence time in Hog Island Bay, located at the center of the Virginia Coast Reserve (USA). Residence time in the lagoon was found to be sensitive to variations in wind, tidal range, and tidal stage. Moreover, their results

52 revealed that in lagoons regulated by shallow friction the residence time has low values near the
53 inlets, while it becomes higher near the mainland. Safak et al. [2015] found that the residence
54 time near the inlets is influenced by the tidal phase at the moment of particles release, whereas it
55 is affected by wind in the inner parts of the bay. Finally, the exchange of water volume in the
56 same bays was derived from remote sensing images and in situ tracers by Allen et al. [2011].
57 They found that about half of the water volume is flushed out of the bay during each tide cycle,
58 while the other half is left inside the system and it is exported at a slower rate.
59 However, a comprehensive and systematic analysis of all processes determining the flushing of
60 a tracer is still lacking. The main purpose of this study is to understand the hydrodynamic
61 conditions under which a tracer is flushed out at the fastest rate. Particular attention is devoted to
62 water circulation induced by wind and variations in tidal phase and amplitude along the shelf,
63 which are shown to be the most effective processes flushing this system.
64 We compute the flushing time of the bays in order to compare different physical drivers.
65 Flushing time, water age, exposure time, and residence time are timescales that describe the
66 exchange and transport of water and dissolved materials in a coastal sea [Rayson et al., 2016;
67 Monsen et al., 2002; Takeoka, 1984]. The residence time quantifies the retention time of water
68 within a defined control volume, and it is a frequently used metric to evaluate the transport of
69 substances [Braunschweig et al., 2003] and to determine the ability of tides to remove pollutant
70 from a semi-enclosed water body [Patgaonkar et al., 2012]. This parameter depends on tidal
71 range, bathymetry, stratification, wind, and freshwater runoff and is considered to be a local
72 measure that varies in time [Choi and Lee, 2004]. Another commonly used transport time scale is
73 the flushing time which measures the average time that water and its constituents spend within a
74 reservoir before being flushed out [Du et al., 2018]. Flushing time is a bulk parameter that
75 quantifies the overall flushing of the system, and it only describes the renewal capability of a
76 waterbody without taking into account the physical processes that regulate the exchange of
77 material and their spatial distribution [Du et al., 2018; Rayson et al., 2016; Monsen et al., 2002].
78 The second goal of the paper is to determine whether tidal prism and variations in tidal phase
79 and amplitude at the inlets control the flushing time of the bays. A higher tidal prism during
80 spring tides or wind setup increases the exchange of water between bays and the ocean, likely
81 exporting more tracer. Tidal phase differences along the coast lead to asymmetric fluxes,
82 promoting tracer flushing. This is because a tidal phase lag between inlets produces surface

water gradients in the bays that drive residual circulation. This residual circulation decreases flushing time [Herrling and Winter, 2015].

The third goal of this paper is to reduce the description of the system dynamics to a single-parameter model, in order to facilitate the comparison of flushing time values under different external agents. A single-parameter model allows the fast determination of flushing time as a function of tidal and wind conditions without the need of expensive 2D simulations. Lagrangian (particle tracking) and Eulerian (tracer patch) methods are typically used to analyze transport time scales in estuaries. The Lagrangian approach explicitly simulates the trajectories of individual tracer particles and registers the time when they leave the domain providing spatial and temporal variations in residence time; the residence time is defined for each water parcel, and this approach is thus frequently employed to relate the time-varying position of particles to the point of their initial release [Rayson et al., 2016; Andutta et al., 2013; Braunschweig et al., 2003; Monsen et al., 2002]. On the other hand, the Eulerian approach might be more suitable for the residence time evaluation in the entire domain [Aikman and Lanerolle, 2004]. Eulerian formulations can be more easily translated into a single-coefficient parametrization to describe the decay of mass within a lagoon [Cucco et al., 2009]. Moreover, the Eulerian approach properly models the advection and diffusion processes [Deleersnijder et al., 2001]. Flushing time can also be estimated with the freshwater fraction method. This approach involves the calculation of the total volume of freshwater found in an estuary and it estimates the flushing time as the time taken to replace the existing freshwater in the estuary at the same rate of the freshwater input [Guo and Lordi, 2000; Williams, 1986; Dyer, 1973]. The application of the Lagrangian and Eulerian methods to study the hydrodynamics of lagoons and the relationship to particle residence time has been presented in several studies. Safak et al. [2015] used the Lagrangian particle tracking method to evaluate both the residence time of neutrally buoyant particles and their exchange between the bays of the Virginia Coast Reserve system. The residence time obtained with this approach was low, varying from a few hours to a few weeks depending on the release location; this result was probably due to a relatively short simulation period (two months), and to the fact that residence time estimates the time particles need to reach the boundary of the domain without reentering once they exit the inlets. Defne and Ganju [2014] employed a Lagrangian model for the analysis of particle trajectories and employed different methods for the evaluation of the residence time in an estuary. They found that, when the

simulation period is too short, the residence time given by ensemble averaging the residence time of each particle in the domain does not account for the particles that remain in the domain. Burwell et al. [2000] compared the Eulerian and Lagrangian methods in predicting the residence time of neutrally buoyant particles in a bay. The Eulerian method gave a good description of the residence time variations in the bay, but it was affected by diffusion which produced lower residence times compared to those produced by the Lagrangian method. In addition, the Lagrangian approach was better suited to describe the spatial distribution of residence time, but it presented limitations due to its sensitivity to the number of particles simulated in the model and the eddy diffusivity value, which is set a priori and it is assumed to remain constant in time. Delhez and Deleersnijder [2006] developed an Eulerian procedure that is equivalent to the Lagrangian method and allows estimation of residence time as a function of space and time. This adjoint method presents the advantage of delineating the fine spatial distribution of the particles in the domain in space and time, while reducing the difficulties associated with the Lagrangian representation of a spatially variable diffusivity.

Herein, we follow results from Cucco et al. [2009] who state the Eulerian approach is more suitable to investigate the long-term flushing of substances from a tidal embayment. We evaluate the fluxes of a conservative tracer within a system of shallow coastal bays along the Atlantic coast of the USA, in the Virginia Coast Reserve (VCR). The transport of the tracer and its flushing time are examined under different external forcing conditions, such as of tides and wind induced currents. The tidal flow and the circulation of water and tracer are simulated using the hydrodynamic model Delft3D-FLOW [Lesser et al., 2004; Roelvink and Van Banning, 1994]. The Eulerian method is applied to evaluate the time evolution of the spatially-averaged flushing time.

2 Study area

The Virginia Coast Reserve (VCR) is a system of shallow coastal bays that extends for 100 km along the Atlantic Coast of the southern portion of the Delmarva Peninsula, USA (Figure 1).

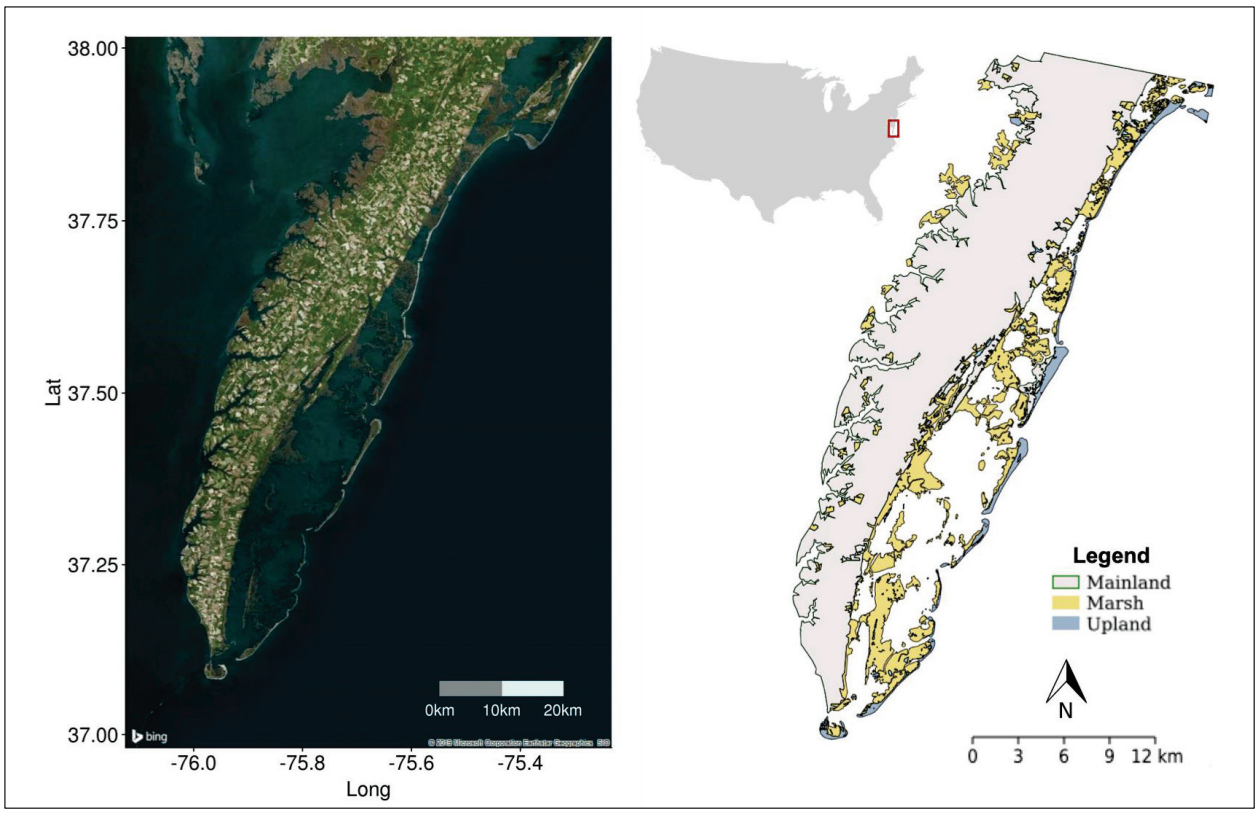

Figure 1. On the left, Virginia Coast Reserve along the Delmarva Peninsula. On the right, main land cover types found in the study area (https://www.vcrlter.virginia.edu/home2/).

The peninsula is bounded by Chesapeake Bay to the West and by the Atlantic Ocean to the East. VCR includes 14 barrier islands protecting bays of different size. The small watersheds found in the upland part of the study area supply a negligible amount of fluvial freshwater and sediment to the lagoons [Nardin et al., 2018; Wiberg et al, 2015; Fugate et al., 2006], and the water fluxes among different bays as well as the connection between bays and the ocean varies significantly within the system [Wiberg et al., 2015]. The shallow bays present an average depth of 1.0 m below mean sea level and are connected to the Atlantic Ocean by a network of channels which have a mean depth of 5 m and become more than 10 m deep at the inlets [Nardin et al., 2018, Mariotti et al., 2010]. Tides are semidiurnal and the mean tidal range is about 1.2 m [Safak et al., 2015]. The principal wind directions are from SSE-SSW and N-NE and the highest wind speeds are observed during the winter season [Fagherazzi and Wiberg, 2009].

Freshwater inputs to the VCR bays are minimal, and measurements of freshwater discharge in three representative streams (out of 54) indicate an average discharge of 0.03 m^3/s in each stream

158 [Anderson et al., 2009], so that the estimated total freshwater flux to the bays is less than 0.3%
159 the tidal prism. As a result, salinity variations in the bays are negligible. Salinity measurements
160 along two transects that run from the inlet to the mainland in the southern part of the Delmarva
161 Peninsula indicate average salinity of 31.0 ± 1.7 and 31.0 ± 1.1 ppt at the inlets, and 29.7 ± 2.7
162 and 29.0 ± 3.8 ppt at the landward shore of the bay [McGlathery et al. 2018]. Tidal exchange
163 dominates transport processes in these bays and it has been the subject of previous studies [e.g.
164 Wiberg et al., 2015; Fagherazzi and Wiberg, 2009; Fugate et al., 2006], but many mechanisms,
165 such as those responsible for the flushing of pollutants and temporal variations in flushing time,
166 remain unclear.

167 **3 Methods**

168 3.1 Model description

169 The hydrodynamic model Delft3D-FLOW [e.g. Lesser et al., 2004; Roelvink and Van
170 Banning, 1994] was used to reproduce the hydrodynamics and transport of tracers in the VCR
171 bays under tidal and wind forcing. The domain of the study area was delineated by a numerical
172 grid of dimension 459x200, and cell size of 250x250m. Three open boundaries were defined
173 along the East (Atlantic Ocean), South, and North sides of the domain (Figure 2). Given that
174 VCR has no significant fluvial sources of freshwater and the salinity is overall uniform, the
175 domain of the study area was composed of one vertical layer (2D), as in several other previous
176 studies conducted over the same region [Nardin et al., 2018; Wiberg et al., 2015; Mariotti et al.,
177 2010].
178 The water level was defined on all open boundaries by superimposing the various tidal
179 harmonics with their corresponding phases and amplitudes. In a first set of simulations we used
180 as boundary conditions the tidal harmonics obtained from the NOAA Wachapreague Station
181 (8631044, Wachapreague, Virginia, USA). The amplitude and phase were adjusted to account
182 for the propagation and amplification/dissipation of the tide in the lagoons and to properly
183 reproduce the measured tides at the location of the Wachapreague station.
184 In a second set of simulations the phase and amplitude were assumed to vary along the open
185 boundaries in order to account for spatial differences of the tidal signal in the Middle Atlantic
186 Bight. These differences were small, but they can affect residual tidal currents. Specifically, the
187 North and South boundaries (Figure 2) were divided into five segments, while the Atlantic

188 boundary was split into 10 segments. The amplitude and phase of the end points of each segment
189 were derived from the ADCIRC Tidal Database for the Atlantic Ocean [Mukai et al., 2002], and
190 then linearly interpolated by Delft3D so that the model could reproduce the regional tidal
191 forcing.
192 The presence of vegetation was accounted by means of a spatially varying Chezy coefficient
193 for bed roughness. The coefficient was set equal to 65 $m^{1/2}/s$ in the marshes and 45 $m^{1/2}/s$ in the
194 rest of the grid [Safak et al. 2015; Wiberg et al. 2015]. The tracer introduced in the model was
195 non-active and had no settling velocity. Sediment transport processes, as well as possible
196 morphological changes were neglected. The initial tracer concentration was equal to one at every
197 grid cell of the domain inside the lagoons and to zero for ocean and upland cells, with a clamped
198 condition (zero tracer concentration) at the boundaries.
199 When wind is present, a spatially constant wind speed was applied to the entire domain. The
200 wind exerts drag that was implemented as a surface shear stress term in the momentum
201 equations. The magnitude of the shear stress was computed as $\tau = \rho C_d U_{10}^2$, where U_{10} is the wind
202 speed 10 meter above the free surface, ρ the density of air, and C_d the wind drag coefficient,
203 which was assumed not to vary with wind speed and to be equal to 0.00723.

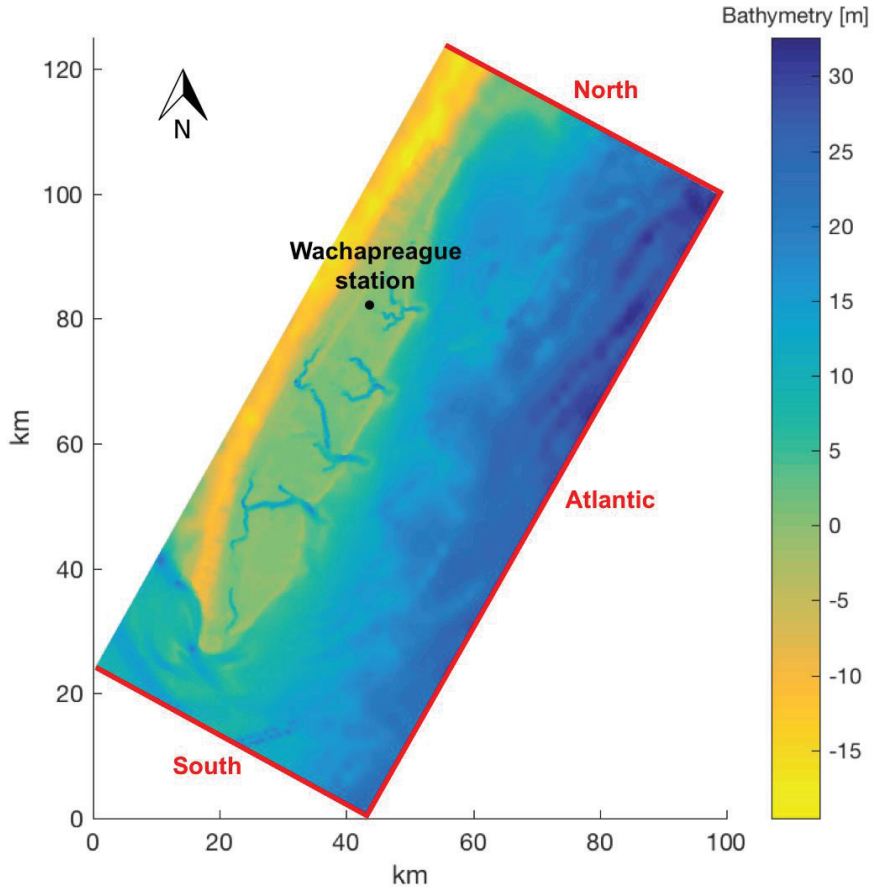

Figure 2. Bathymetry, boundaries of the domain of the study area, and location of NOAA Wachapreague station (8631044, Wachapreague, Virginia, USA).

3.2 Model validation

Following Cunge [2003], model calibration relies on careful adjustment of the tidal boundary conditions. This is consistent with the results of Abbott and Cunge [1975] who showed that adjusting the boundary conditions, rather than adjusting friction, was a more reliable approach to the calibration of estuarine models. The same approach was adopted by Wiberg et al. [2015] and Mariotti et al. [2010] for the VCR bays. The calibration of the boundary conditions was done by comparing simulated water levels with water levels measured at Wachapreague station, for the period from April 1st (time 00:00:00) to April 5th, 2015 (time 00:00:00). The model performance was evaluated with two statistics: the model efficiency, ME, and the root mean squared error, RMSE [Mariotti et al., 2010]. Both phase and amplitude at the boundaries were varied until reaching the maximum model efficiency. The values calculated were 0.97 for ME and 0.26 m for RMSE. The amplitude and phase at Wachapreague station before (observed values) and after the

calibration (calibrated values) are presented in Table S1.

To test the reliability of the model we computed the difference in amplitude and phase between the main harmonic constituents measured by NOAA at the Wachapreague station and the harmonic constituents simulated by Delft3D with the ADCIRC boundary conditions (Figure S1). The extraction of the harmonic constituents from the modeled water level was carried out using the T_tide Harmonic Analysis Toolbox [Pawlowicz et al., 2002]. The model validation gave excellent results, with amplitude differences of less than 2 cm and phase differences of less than 12 degrees (*VARYING TIDE* scenario, Figure S1). For comparison, we also plotted the difference in amplitude and phase using the modified Wachapreague tidal signal along all boundaries (*SPRING&NEAP* tide scenario, Figure S1). This model performed very well, although it led to slightly higher phase errors due to the neglect of phase variations along the Atlantic boundary.

3.3 Simulation scenarios

The performed simulations are meant to explore whether the flushing time and the decay of the tracer can be altered by one the following: i) differences in the time of release of the tracer with respect to the tidal cycle, ii) tidal amplitude, iii) variations in tidal phase and amplitude along the inner shelf, iv) shelf currents and varying tide along the boundaries, and v) wind conditions.

To study whether differences in the time of release affect the flushing of the tracer, a base scenario, called standard simulation (*STD*), was run based on the average values of tidal amplitude and frequency of the first six harmonics (M2, S2, N2, K1, M4, O1) at the open boundaries. The same simulation was run twice, once starting from ebb conditions (*STD EBB*) and once starting from flood conditions (*STD FLOOD*). For both cases, the initial water level was around mean sea level. In a second set of simulations the tracer was released in correspondence of high (*HIGH WL*) and low tide (*LOW WL*) at the open boundaries.

To determine whether tidal amplitude affects flushing time, we ran a simulation with the smallest amplitude associated to the N2 constituent, called *N2 AMPLITUDE*, and another simulation with tidal amplitude equal to the sum of the amplitudes of the harmonic constituents, combined to obtain the maximum tidal amplitude (*MAX AMPLITUDE*). Tidal amplitudes that are much different from the measured ones are unrealistic. However, we chose to run these hypothetical scenarios in order to expand the parameter space of the simulations, so that we can better understand the processes controlling the flushing of a tracer. Other two simulations were

run by accounting for the gradual alternation between the spring and neap tide, given by the combination of the first six harmonics (M2, S2, N2, K1, M4, O1). In one of these, the tracer was released during spring tide (*SPRING&NEAP*), and in the other the tracer was released during neap tide (*NEAP&SPRING*).

To account for the spatial variation of the amplitude and frequency of each harmonic constituent along the Virginia shelf we simulated the tracer mass decay under the effect of a realistic tidal forcing (*VARYING TIDE*). To determine the effect of currents on flushing time, we run a simulation (*CURRENT*) where we added a shelf current of 3 cm/s moving from northeast to southwest along the shore. The current velocity was imposed perpendicular to the north and south boundaries and was derived from field measurements of circulation over the Middle Atlantic Bight continental shelf [Lentz 2008].

To determine the effect of wind on flushing time, we run twenty-one simulations with a wind with constant speed and direction. Eight wind directions (every 45°, with north equal to 0°), and four values of wind speed, 5, 6, 10 and 12 m/s, were considered. The convention used to name each of the simulations that involve the wind effect is the following: the first part of the name is determined by the direction (e.g. the wind blowing from south is called *S*, and the wind coming from south-east is called *SE*), while the second part of the name is the wind speed in m/s (e.g. the wind blowing from north-west with a velocity of 5 m/s is labeled as *NW5*). *No Wind* indicates the scenario without wind. The characteristics of all the scenarios simulated in this study are described in Table 1. Wind constantly blowing from one direction for several weeks is unrealistic. Similarly to Scully et al. [2013], we also ran two simulations including wind data observed at the NOAA Wachapreague station during the winter and summer seasons of 2015 (*WINTER WIND* from December 21st, 2014 to March 20th, 2015, and *SUMMER WIND* from June 21st to September 23rd, 2015). The measured wind data (Figure 3) in the summer period included a block of missing values from September 1st to September 9th and these data were ignored in the evaluation of the decay parameter. No wind was prescribed during such period. All of the above simulations started at mean sea level during ebb, with the exceptions of the low and high water level ones.

278 **Table 1.** Parameters of the scenarios simulated with Delf3D.

279

Simulation ID	Initial time	Final time	Amplitude and Phase	Wind direction [°]	Wind speed [m/s]
STD EBB	01/04/2015 03:18 (MSL, ebb)	01/08/2015 03:18m	Average amplitude*, null phase	-	-
STD FLOOD	01/04/2015 21:19 (MSL, flood)	01/08/2015 21:19m	Average amplitude*, null phase	-	-
HIGH WL	01/04/2015 00:12 (High tide, ebb)	01/08/2015 00:12 m	Average amplitude*, null phase	-	-
LOW WL	01/04/2015 06:19 (Low tide, ebb)	01/08/2015 06:19m	Average amplitude*, null phase	-	-
MAX AMPLITUDE	01/04/2015 04:24 (MSL, ebb)	01/08/2015 04:24m	Sum of amplitudes**, null phase	-	-
N2 AMPLITUDE	01/04/2015 03:13 (MSL, ebb)	01/08/2015 03:13m	N2 amplitude, null phase	-	-
SPRING&NEAP	18/04/2015 17:23 (MSL, ebb)	18/08/2015 17:23m	M2, S2, N2, K1, M4, O1	-	-
NEAP&SPRING	12/04/2015 05:48 (MSL, ebb)	12/08/2015 05:48m	M2, S2, N2, K1, M4, O1	-	-
VARYING TIDE	01/04/2015 02:47 (MSL, ebb)	01/08/2015 02:47m	M2, S2, N2, K1, M4, O1 from ADCIRC	-	-
CURRENT	01/04/2015 02:47 (MSL, ebb)	01/08/2015 02:47m	M2, S2, N2, K1, M4, O1 from ADCIRC	-	-
SE6	01/04/2015 03:08 (MSL, ebb)	01/08/2015 03:08m	Average amplitude*, null phase	135	6
SE12	01/04/2015 02:29 (MSL, ebb)	01/08/2015 02:29m	Average amplitude*, null phase	135	12
SW6	01/04/2015 03:19 (MSL, ebb)	01/08/2015 03:19m	Average amplitude*, null phase	225	6
SW12	01/04/2015 03:28 (MSL, ebb)	01/08/2015 03:28m	Average amplitude*, null phase	225	12
NO WIND	21/06/2015 00:00 (MSL, ebb)	23/09/2015 23:00m	M2, S2, N2, K1, M4, O1	-	-

[

N5	21/06/2015 00:00 (MSL, ebb)	23/09/2015 23:00m	M2, S2, N2, K1, M4, O1	0	5
N10	21/06/2015 00:00 (MSL, ebb)	23/09/2015 23:00m	M2, S2, N2, K1, M4, O1	0	10
NE5	21/06/2015 00:00 (MSL, ebb)	23/09/2015 23:00m	M2, S2, N2, K1, M4, O1	45	5
NE10	21/06/2015 00:00 (MSL, ebb)	23/09/2015 23:00m	M2, S2, N2, K1, M4, O1	45	10
E5	21/06/2015 00:00 (MSL, ebb)	23/09/2015 23:00m	M2, S2, N2, K1, M4, O1	90	5
E10	21/06/2015 00:00 (MSL, ebb)	23/09/2015 23:00m	M2, S2, N2, K1, M4, O1	90	10
SE5	21/06/2015 00:00 (MSL, ebb)	23/09/2015 23:00m	M2, S2, N2, K1, M4, O1	135	5
SE10	21/06/2015 00:00 (MSL, ebb)	23/09/2015 23:00m	M2, S2, N2, K1, M4, O1	135	10
S5	21/06/2015 00:00 (MSL, ebb)	23/09/2015 23:00m	M2, S2, N2, K1, M4, O1	180	5
S10	21/06/2015 00:00 (MSL, ebb)	23/09/2015 23:00m	M2, S2, N2, K1, M4, O1	180	10
SW5	21/06/2015 00:00 (MSL, ebb)	23/09/2015 23:00m	M2, S2, N2, K1, M4, O1	225	5
SW10	21/06/2015 00:00 (MSL, ebb)	23/09/2015 23:00m	M2, S2, N2, K1, M4, O1	225	10
W5	21/06/2015 00:00 (MSL, ebb)	23/09/2015 23:00m	M2, S2, N2, K1, M4, O1	270	5
W10	21/06/2015 00:00 (MSL, ebb)	23/09/2015 23:00m	M2, S2, N2, K1, M4, O1	270	10
NW5	21/06/2015 00:00 (MSL, ebb)	23/09/2015 23:00m	M2, S2, N2, K1, M4, O1	315	5
NW10	21/06/2015 00:00 (MSL, ebb)	23/09/2015 23:00m	M2, S2, N2, K1, M4, O1	315	10
WINTER WIND	21/12/2014 00:00 (MSL, ebb)	20/03/2015 23:00m	M2, S2, N2, K1, M4, O1	Observed data	Observed data

[

SUMMER WIND	21/06/2015 00:00 (MSL, ebb)	23/09/2015 23:00m	M2, S2, N2, K1, M4, O1	Observed data	Observed data

* Average value of the amplitudes of the first six harmonic constituents, equal to 0.139425 m

** Sum of the amplitudes of the first six harmonic constituents, equal to 0.83655 m

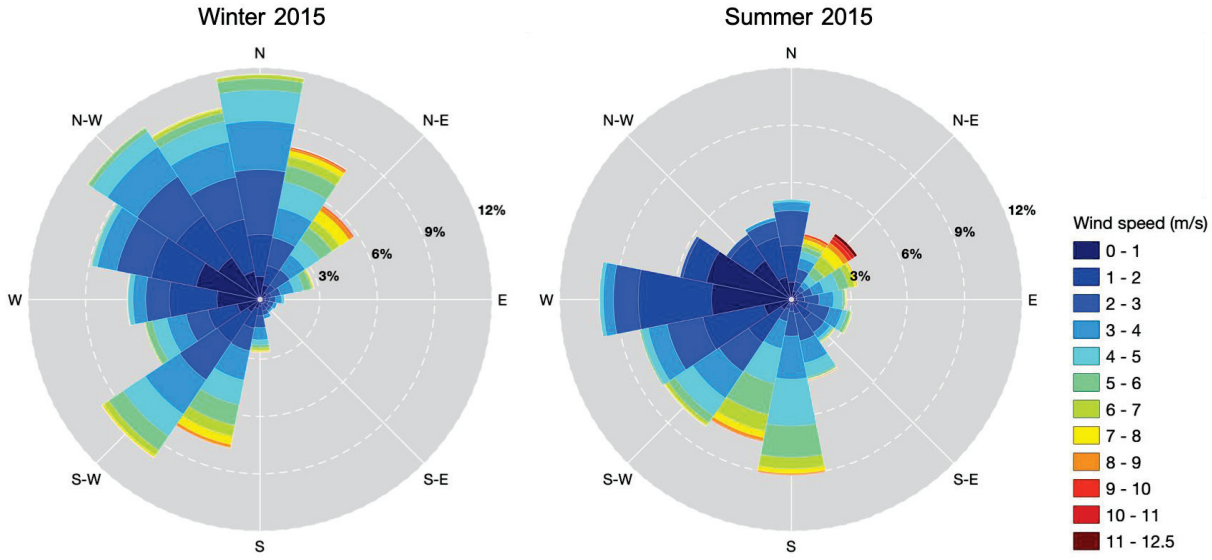

Figure 3. Distribution of wind speed and direction observed at NOAA Wachapreague station, Virginia, USA (tidesandcurrents.noaa.gov). On the left, the winter season from December 21st, 2014 to March 20th, 2015. On the right, the summer season from June 21st to September 23rd, 2015. Colors indicate the wind speed, as specified in the legend. The radial axis shows the frequency expressed as percentage of the total measurements of each combination of wind speed and direction.

3.4 Decay of tracer concentration and flushing time

The flushing time is a system-level measure that quantifies the effectiveness of tidal flushing in removing a dissolved substance from a water body through its open boundaries and provides a single value for the whole system [Choi and Lee, 2004]. A water body connected to the sea, such as a coastal embayment, is characterized by a flushing time that is well approximated by a double-exponential decay curve [Defne and Ganju 2014; Periáñez et al. 2013; Choi and Lee, 2004]. In this study the time variation of the tracer mass fraction that remains in the lagoon in the absence of wind was approximated with a double-exponential function as it presents higher

299 correlation coefficients compared to a single exponential curve. The interpolation was
300 implemented on the curve obtained by averaging the mass fraction within the system of bays
301 every tidal cycle, as shown in Figure 4.
302

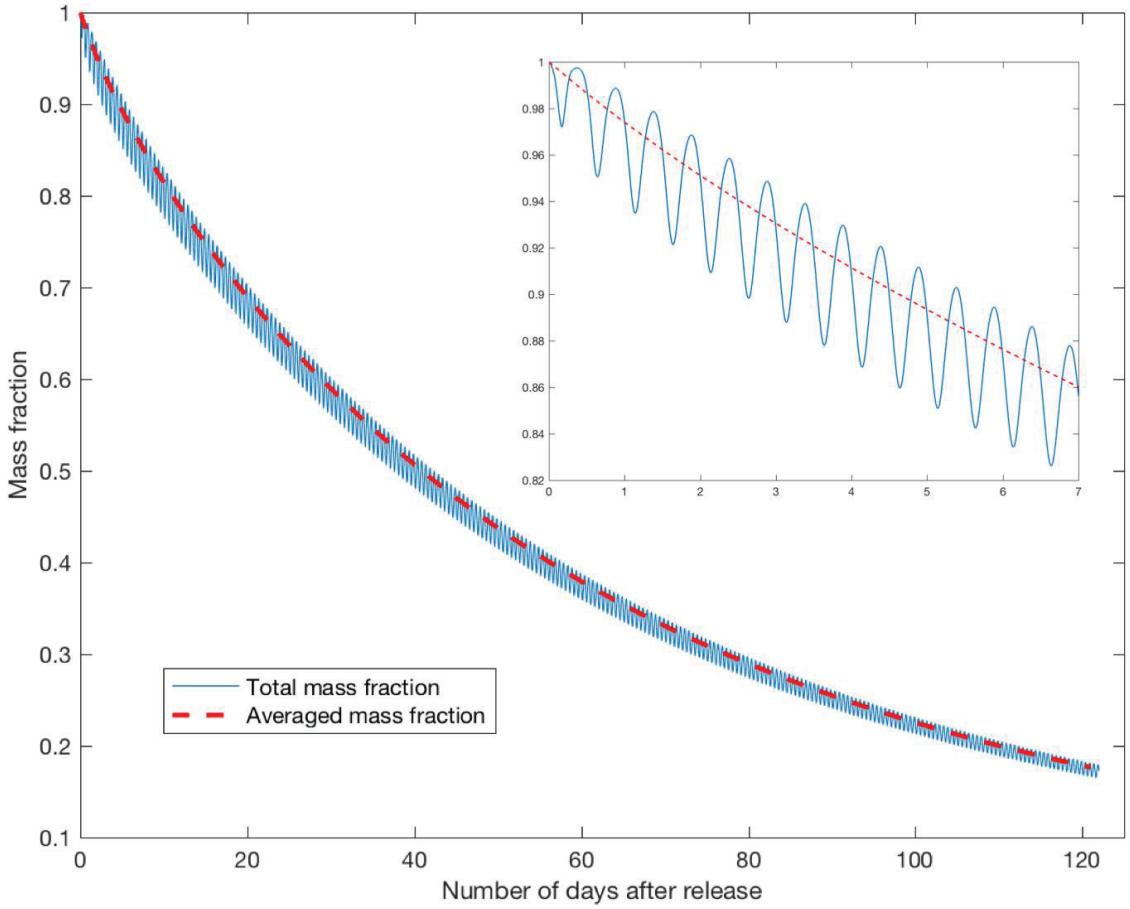

303
304 **Figure 4.** Mass fraction decay for the *STD EBB*. The blue line represents the decaying mass
305 fraction calculated as integral over the entire bay. The red line is the corresponding average. In the
306 smaller panel a magnification of the first simulation days is reported.
307
308 The decay function is made of two exponential terms, and is defined by the three parameters
309 a, b, c:
310

311 $$\frac{m(t)}{m_0} = ae^{-bt} + (1-a)e^{-ct} \quad (1)$$

312

where $m(t)$ is the tracer mass at time t, m_0 is the tracer initial mass. This function describes a decay process that is faster at the beginning and gets slower with time [Defne and Ganju, 2014]. The corresponding flushing time, T_f, was determined using the following equation [Choi and Lee, 2004]:

$$T_f = \frac{a}{b} + \frac{1-a}{c} \quad (2)$$

When a strong, constant wind is included in the model, the flushing process is faster, and the flushing time obtained from a single-exponential curve is similar to the value obtained from a double-exponential curve (Table S2). Therefore, in the simulations including wind, the decay of the tracer mass was interpolated with a simple exponential curve:

$$\frac{m(t)}{m_0} = ke^{-\lambda t} \quad (3)$$

where k (≈1) and λ are the parameters of the exponential function. In this case, the decay rate λ was employed to evaluate the flushing time, T_f, of the tracer [Choi and Lee, 2004]:

$$T_f = \frac{1}{\lambda} \quad (4)$$

An example of the different interpolations of the mass decay produced by the single and double exponential functions for the *STD EBB* scenario can be found in Figure S2.

3.5 Velocity skew at the inlets

In order to determine what process is responsible for the flushing of the tracer, the flushing time computed from Equations 2 and 4 was compared to the monthly averaged tidal prism of the bays and the velocity skew at the inlets. The tidal prism accounts for the total amount of water exchanged in a tidal cycle between the bays and the ocean. A larger tidal prism means larger fluxes and possibly a decrease in flushing time. The velocity skew at each inlet however accounts for the asymmetry of the tidal flow. Ebb velocities greater than flood velocities would prevent the return of the tracer into the bays, reducing the flushing time. This is particularly true

for a bay with several inlets, in which water can enter from one inlet during flood but then exits from a different inlet during ebb. Following Nidzieko and Ralston [2012], the velocity skew is computed as:

$$S = \frac{\int_0^T v^3 dt}{\left(\int_0^T v^2 dt\right)^{3/2}} \quad (5)$$

where v is the maximum velocity in the inlet and T is the tidal period.

We also defined a total skew index, which accounts for the combined skew of each inlet and provides a metric of asymmetry for the entire complex of bays:

$$S_{tot} = \sum_1^n |S_i| \quad (6)$$

where S_i is the velocity skew of one inlet and n is total number of inlets.

3.6 One-dimensional model for computing flushing time under different wind conditions

Simulations with constant wind speed and direction were used to construct a polynomial function that allows the determination of the exponential decay of the tracer mass using the least number of parameters. The goal of this method is to collapse complex, time-consuming 2D simulations in a simple point model based on a parameterized polynomial. This simple point model can then be effectively used to rapidly determine the flushing time of the system as a function of wind conditions.

In the presence of wind, the decay parameter λ was evaluated as a function of wind direction and wind speed. Specifically, the wind speed, $v\ (m/s)$, and direction, $\theta\ (rad)$, and the corresponding decay rate, λ, for the exponential curve (Equation 3) were related using the following polynomial regression function:

$$\lambda(\theta, v) = p_1 + p_2\theta + p_3 v + p_4\theta^2 + p_5\theta v + p_6 v^2 + p_7\theta^3 + p_8\theta^2 v + p_9\theta v^2 + p_{10}\theta^4 + p_{11}\theta^3 v + p_{12}\theta^2 v^2 \quad (7)$$

where p_1, p_2, p_3, p_4, p_5, p_6, p_7, p_8, p_9, p_{10}, p_{11}, and p_{12} are the coefficients of the interpolating function. This polynomial model presents 4 degrees in the θ variable and 2 degrees

in the v variable, and is the regression function that gave the best fit. Results from these ensemble simulation runs with eight different constant directions and two constant wind speeds were used to determine the coefficients of Equation 5. Specifically, for each simulation a value of λ was determined for the given values of θ and v; these points were then used to fit the polynomial surface represented by Equation 7.

Since the decay exponent was calculated as a function of wind speed and intensity (Equation 7), we could simulate the mass decay for any time period characterized by a variable wind speed. Specifically, we divided the time period in constant intervals, Δt, and for each interval we computed the decay exponent assuming an average wind speed. Then we compounded the results for the whole period. Note that because the decay was exponential, the decay of concentration in time was simply obtained by adding all the exponents:

$$\frac{m(n\Delta t)}{m_0} = ke^{-\sum_1^n \lambda_i \Delta t} \quad (8)$$

where n is the number of time intervals, λ_i is the decay exponent during the interval $i\Delta t$, $(i+1)\Delta t$.

This equation allowed us to reproduce the time-varying mass decay produced by observed values of wind direction and speed. Even if the decay rates for different wind speeds and directions were obtained assuming a constant wind within every time interval, in our model each decay rate is used for only few hours, mimicking the natural wind variability of the Virginia Coast Reserve.

To test the model (Equation 8) we used wind data observed every hour at the Wachapreague station from 21st June to 23rd September 2015 (Figure 3). We derived two additional wind data sets from the hourly observed wind data, by averaging the data every 12 and 24 hours and applying Equation 8 with the same time interval of 12 and 24 hours. The obtained exponential curves were compared to the mass decay determined by a full scale Delft3D simulation during the same time period using the observed water levels and wind data registered at the Wachapreague station.

399 **4 Results**

400 4.1 Factors influencing the flushing time of tracer

401 To determine whether the timing of the tracer injection is important, two standard simulations
402 were carried out, one starting at mean sea level during ebb (*STD EBB*) and one starting at mean
403 sea level during flood (*STD FLOOD*). These two simulations presented a similar decay of the
404 tracer mass (Figure 5a).
405

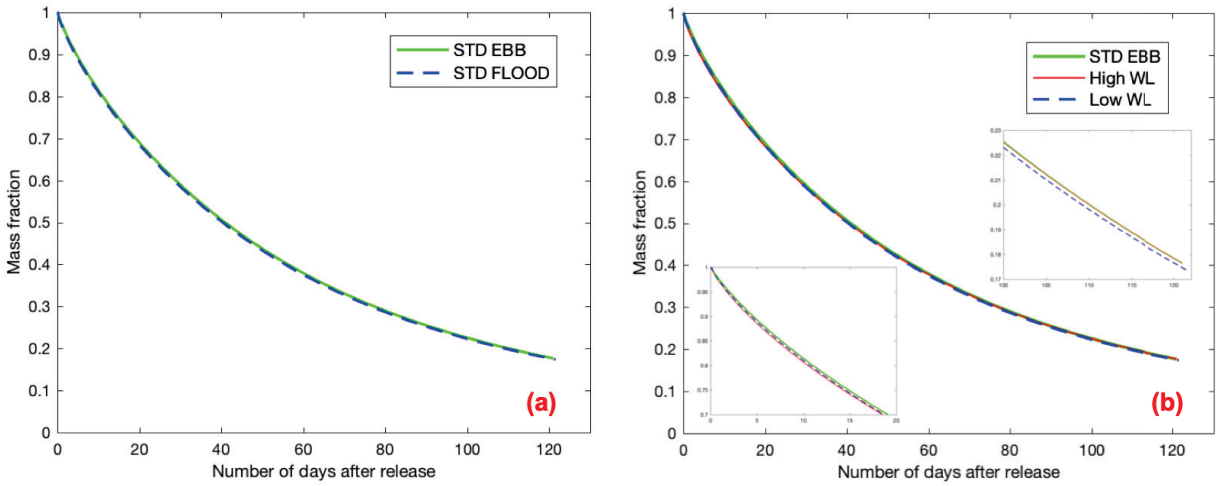

406
407

408 **Figure 5.** (a) Comparison between the mass fraction decay in the simulation for scenarios
409 starting at mean sea level during ebb (*STD EBB*, green line) and at mean sea level during flood
410 (*STD FLOOD*, blue dashed line). (b) Comparison between the mass fraction decay in the
411 simulation starting from mean sea level during ebb (*STD EBB*, green line) and tracer injected
412 during high (*High WL*, red line) and low water level (*Low WL*, blue dashed line). In the inset
413 panels we present a magnification of the first and last days of simulation.
414
415

416 **Table 2.** Values of the coefficients of the double exponential function and flushing time for each
417 simulation without wind. In bold are highlighted simulations that used realistic tide conditions for
418 the VCR bays.
419

[

Simulation ID	a	b ($days^{-1}$)	c ($days^{-1}$)	Flushing time (days)
STD EBB	0.18102	0.05950	0.01294	66.33
STD FLOOD	0.17953	0.06395	0.01306	65.63
HIGH WL	0.16253	0.07537	0.01319	65.68
LOW WL	0.28679	0.03676	0.01175	68.50
MAX AMPLITUDE	0.61253	0.14127	0.02301	21.17
N2 AMPLITUDE	0.12571	0.07032	0.01139	78.55
SPRING&NEAP	**0.43649**	**0.17282**	**0.02500**	**25.06**
NEAP&SPRING	**0.52961**	**0.10923**	**0.02091**	**27.34**
VARYING TIDE	**0.64422**	**0.08857**	**0.02089**	**24.30**
CURRENT	**0.63233**	**0.08474**	**0.01960**	**26.22**

Both simulations had a flushing time of about two months, 66.33 days for *STD EBB* and 65.63 days for *STD FLOOD* (Table 2). This result suggested that there is no significant difference whether a tracer is added to the system during ebb or during flood. In the next two simulations, the initial release of tracer was set to occur during high water level (*HIGH WL*) and low water level (*LOW WL*). Also in this case the flushing time did not show relevant differences (Figure 5b). In addition, the flushing time was similar to the one obtained for the standard simulation starting at mean sea level during ebb; a relatively small (two days) increase in flushing time occurred for the scenario starting at low water level.

Three simulations were then used to investigate the effect of tidal amplitude, and to see whether different tidal ranges influence the flushing time. In the *MAX AMPLITUDE* scenario, the decay of the tracer mass within the lagoon was faster than in the *N2 AMPLITUDE* scenario (Figure 6). The flushing time in the *N2 AMPLITUDE* simulation was about 79 days, approximately 60 days longer than the flushing time computed during the *MAX AMPLITUDE* scenario. Two more simulations were carried out to determine the difference in flushing time under Spring-Neap alternation: in one the tracer was released during a neap tide followed by a spring tide (*NEAP&SPRING*); in the second it was released during a spring tide followed by a neap tide (*SPRING&NEAP*). In this case the comparison presented a less pronounced

438 divergence. The difference in flushing time values was less than 2 days, further demonstrating
439 that the timing of tracer injection had no significant impact in the flushing process (Figure 6).
440

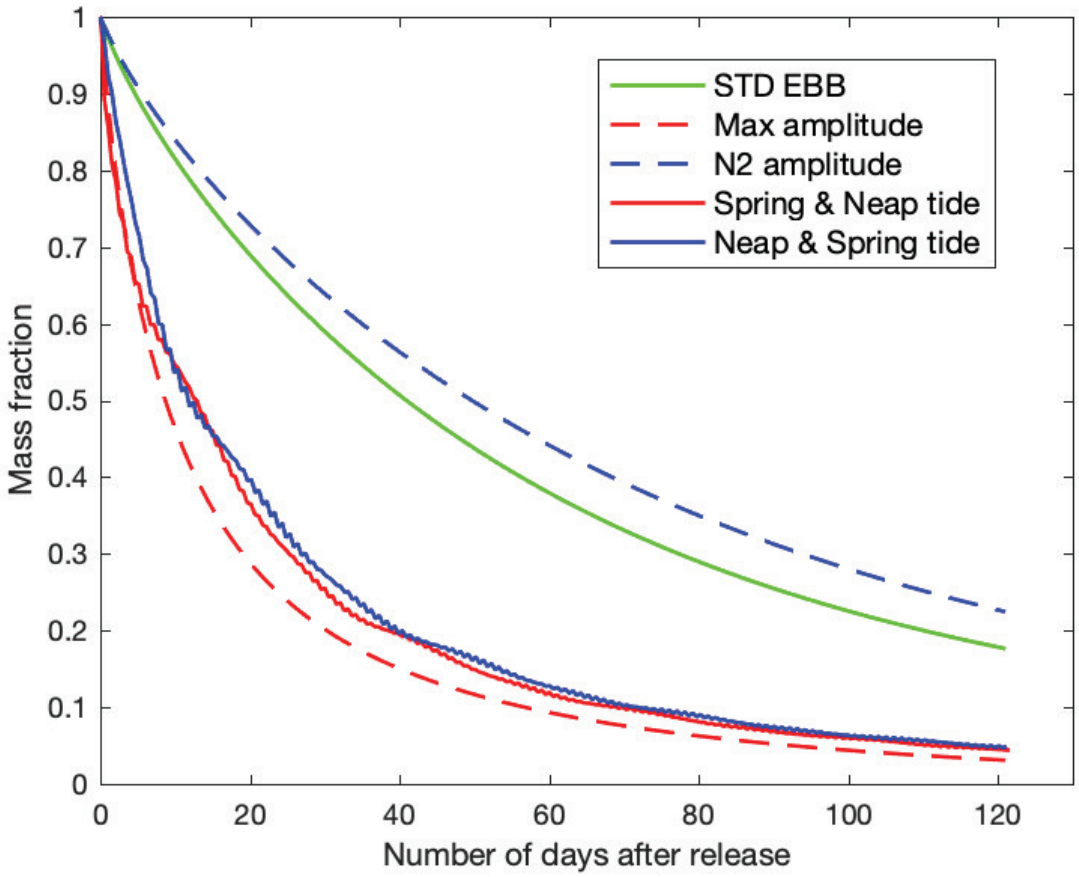

441
442 **Figure 6.** Comparison between the mass fraction decay in the standard simulation and scenarios
443 including Spring and Neap tides. The mass fraction is plotted after one full tide.
444
445 To determine the effect of wind on tracer dispersion, hypothetical simulations with constant
446 wind speed and direction were run. We considered the combination of two wind speeds and two
447 wind directions, one perpendicular and one parallel to the inlets (Figure 7). We chose the two
448 wind directions that produce the maximum (SW) and minimum effect (SE), in order to capture
449 the full variability of this process. In these simulations the decay of the tracer mass fraction
450 resulted to be faster than in the scenarios without wind, indicating that wind might be a strong
451 driver of water exchange in the system. The decay of mass fraction due to the effect of wind can
452 be interpolated with a simple exponential curve, since the use of a double exponential

453 interpolation yields the same values of flushing time and the correlation coefficient is high in
454 both cases (Table S2). Table 3 shows the values of the flushing time evaluated for each
455 simulation using a single exponential function to interpolate the decay. In particular, the
456 simulations with the highest wind speed (12 m/s) were the most effective at flushing the system,
457 and in the case of south-west wind the flushing time reached its lowest value (less than 4 days).
458 Regardless of direction, as the speed doubles its value to 12 m/s, the flushing time decreases and
459 becomes less than half the flushing time obtained when the velocity is 6 m/s.
460

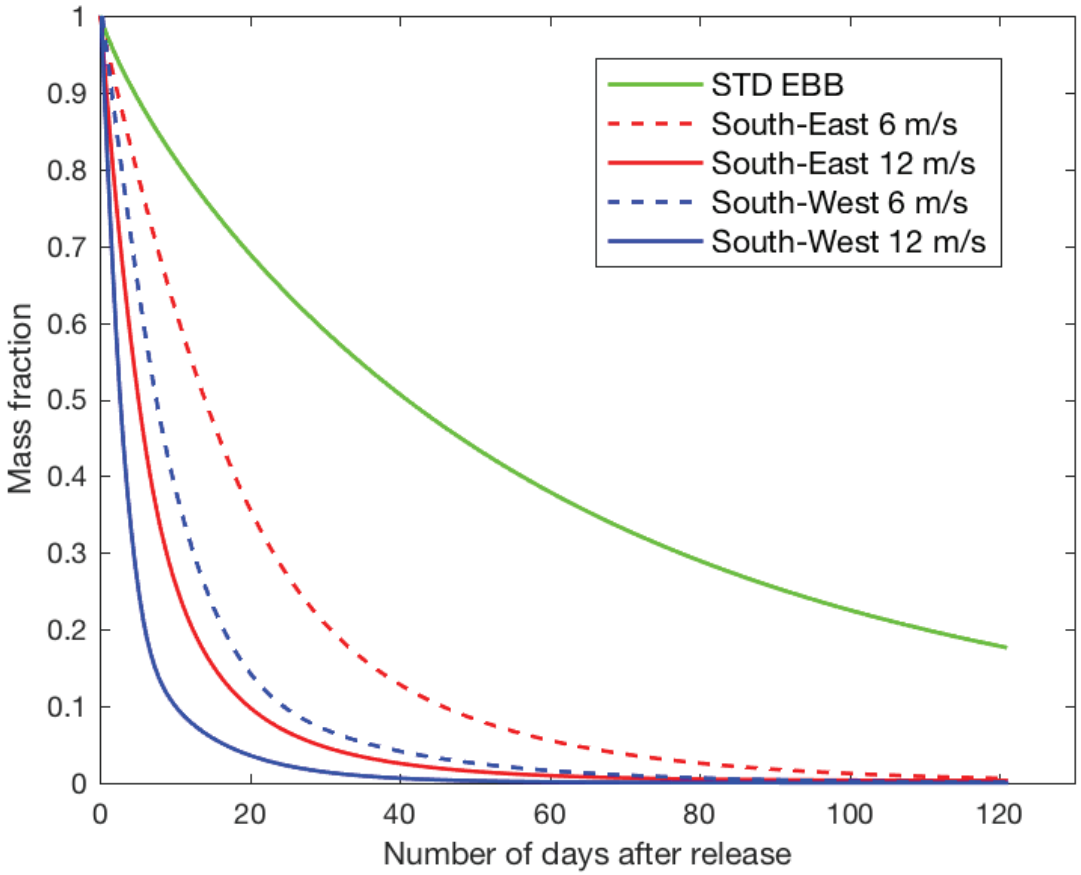

461
462 **Figure 7.** Comparison between the mass fraction decay in the standard simulation and scenarios
463 including wind coming from south-east and south-west directions and with a velocity of 6 m/s and
464 12 m/s.
465
466 However, note that a constant wind lasting for several days is uncommon at the Virginia Coast
467 Reserve, and more realistic conditions with variable wind should also be tested. Two simulations

were run with variable wind conditions measured at Wachapreague (Figure 8). When the variability of wind speed and direction was taken into account, the flushing time increased (Table 3, *WINTER WIND* and *SUMMER WIND* simulations). This is because most of the time the wind is weak (Figure 3). The flushing time computed with winter winds is similar to the flushing time without winds (25.06 days, see Table 3), whereas the flushing time decreases with summer winds to 21.07 days. This is likely due to strong winds from northeast that were present in Summer 2015 (Figure 3).

In the simulation with tidal phasing along the boundary (*VARYING TIDE*) the decay of the tracer concentration in the bays was fast (Figure 8). The flushing time (24.3 days) decreased with respect to *NEAP&SPRING* simulation with a constant phase (27.34 days, see Table 2). This is likely due to subtidal circulation triggered by differences in tidal phase among the inlets. In fact the residual Eulerian velocity enters the bays in the northern inlets, where the tidal signal arrives first, while the velocity exits the bays in the southern inlets, where the tidal signal arrives with a delay (Figure S3). Moreover, at each inlet the residual velocity is segregated in very distinct flood and ebb paths. Both processes increase the dispersion of tracer when it exits the bays, reducing the flushing time.

In the *CURRENT* simulation we considered a current along the shore from northeast to southwest, mimicking the mean shelf circulation over the Middle Atlantic Bight. The flushing time did not further decrease, and instead increased to 26.22 days (Figure 8, Table 2). The four scenarios *VARYING TIDE*, *CURRENT*, *WINTER WIND*, and *SUMMER WIND* used realistic boundary conditions and therefore the corresponding flushing time is more representative of the system.

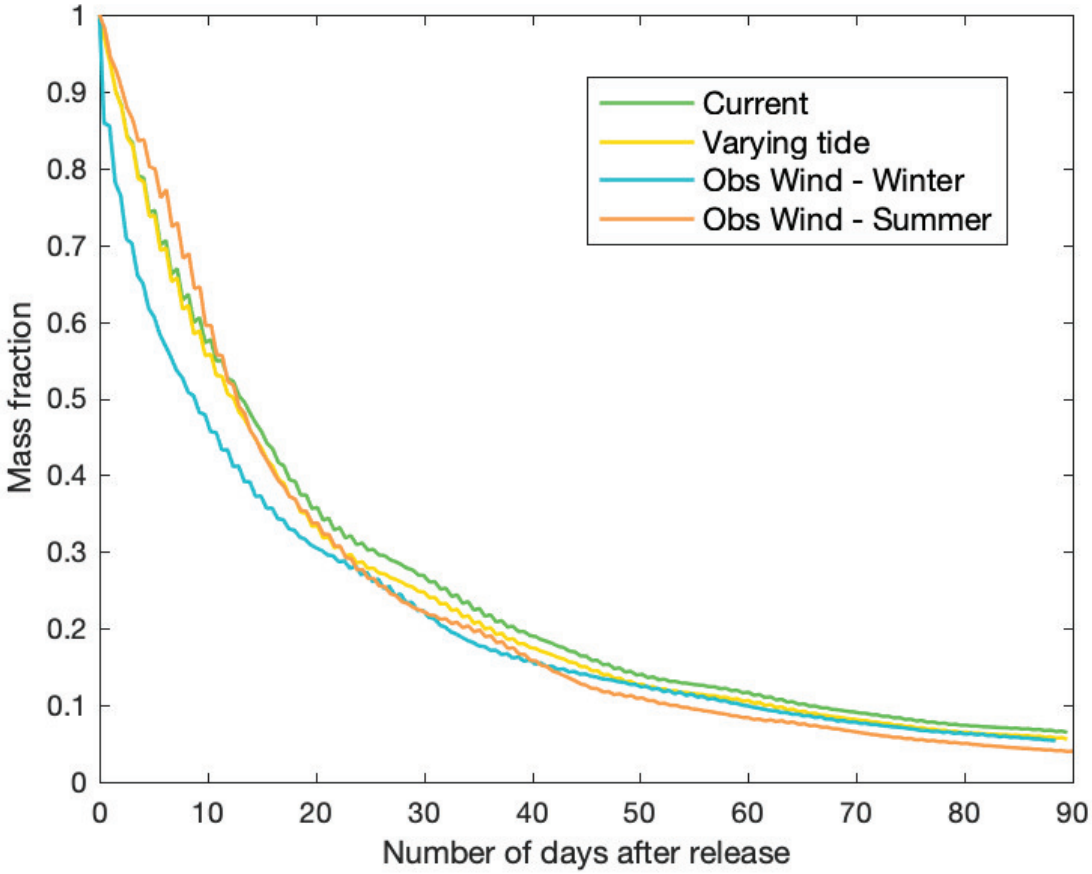

Figure 8. Comparison between the mass fraction decay in the scenario with a shelf current, the scenario with varying tides along the boundaries and the observed wind data in the winter and summer seasons of 2015.

Table 3. Values of the coefficients of the single exponential functions, flushing time, and adjusted R^2 and *RSS* of the interpolation for each simulation including wind. In bold are highlighted simulations that used realistic wind conditions for the VCR bays.

Simulation ID	**K**	**d (days^{-1})**	**Flushing time (days)**	***Adjusted R^2***	***RSS***
SE6	1.0160	0.05112	19.56	0.9990	0.0136
SE12	0.9967	0.12600	7.94	0.9950	0.0420

[

SW6	1.0360	0.09545	10.48	0.9972	0.0278
SW12	1.0230	0.25000	4.00	0.9921	0.0392
WINTER WIND	**0.7568**	**0.03991**	**25.06**	**0.9632**	**0.2266**
SUMMER WIND	**0.9718**	**0.04745**	**21.07**	**0.9874**	**0.1295**

Figure 9 shows the fraction of total concentration of the tracer during the first time steps of the simulation (after 24 and 48 hours on the first day of simulation) in the scenarios without wind (STD EBB) and with wind (south-west 12 m/s and south-east 12 m/s). Both comparisons demonstrate that wind pushes the tracer outside the lagoons and prevents the return of water and tracer inside the lagoons. Therefore, the concentration of tracer remaining in the lagoons decreases if wind is included in the simulation, and as time passes the concentration of tracer decreases faster than in the scenario without wind.

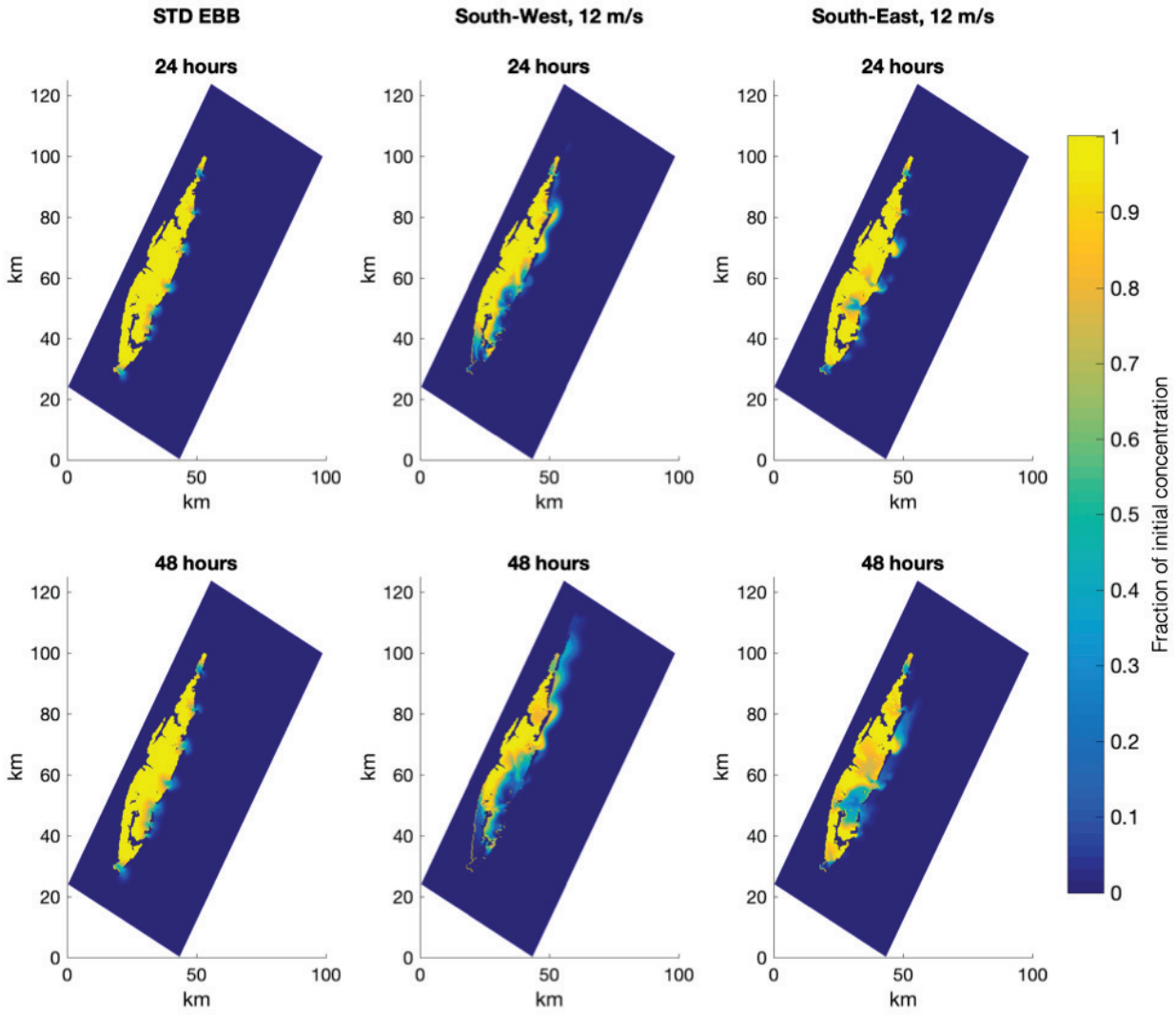

Figure 9. Fraction of total tracer concentration in the lagoon after the first 24 and 48 simulation hours in the scenario without wind (*STD EBB*), and in the scenarios with strong wind (*South-West, 12 m/s*, and *South-East, 12 m/s*).

4.2 Relationship between velocity skew at the inlets and flushing time

We then determined whether tidal prism or velocity asymmetry at the inlets affect the flushing time of tracer in the bays using the results of all simulations. Flushing time is significantly correlated to total skew index (Kendall's tau = -0.73, $p < 0.05$), but not to tidal prism (Kendall's tau = -0.26, $p = 0.06$, Figure 10). Moreover, a multiple linear regression model between the logarithm of the flushing time (response), and the logarithm of the total velocity skew and of the

tidal prism (predictors) has an adjusted R^2 of 0.77 and a *p-value* of 9.88e-09. Specifically, the adjusted R^2 for a linear regression model between the logarithm of the flushing time and the logarithm of the total velocity skew is 0.70 with a *p-value* of 3.37e-08 (see equation in Figure 10). On the contrary, the adjusted R^2 decreases to 0.13 when we analyze the correlation between the flushing time and the tidal prism. These results suggest that the total velocity skew explains 70% of the variance in flushing time in log-log space (Figure 10), while the tidal prism can capture only the 13% of the variance in flushing time; together they explain 77% of the variance in flushing time. The high total skew for the simulations with wind indicates that some of the water entering the system from one inlet exits from a different inlet.

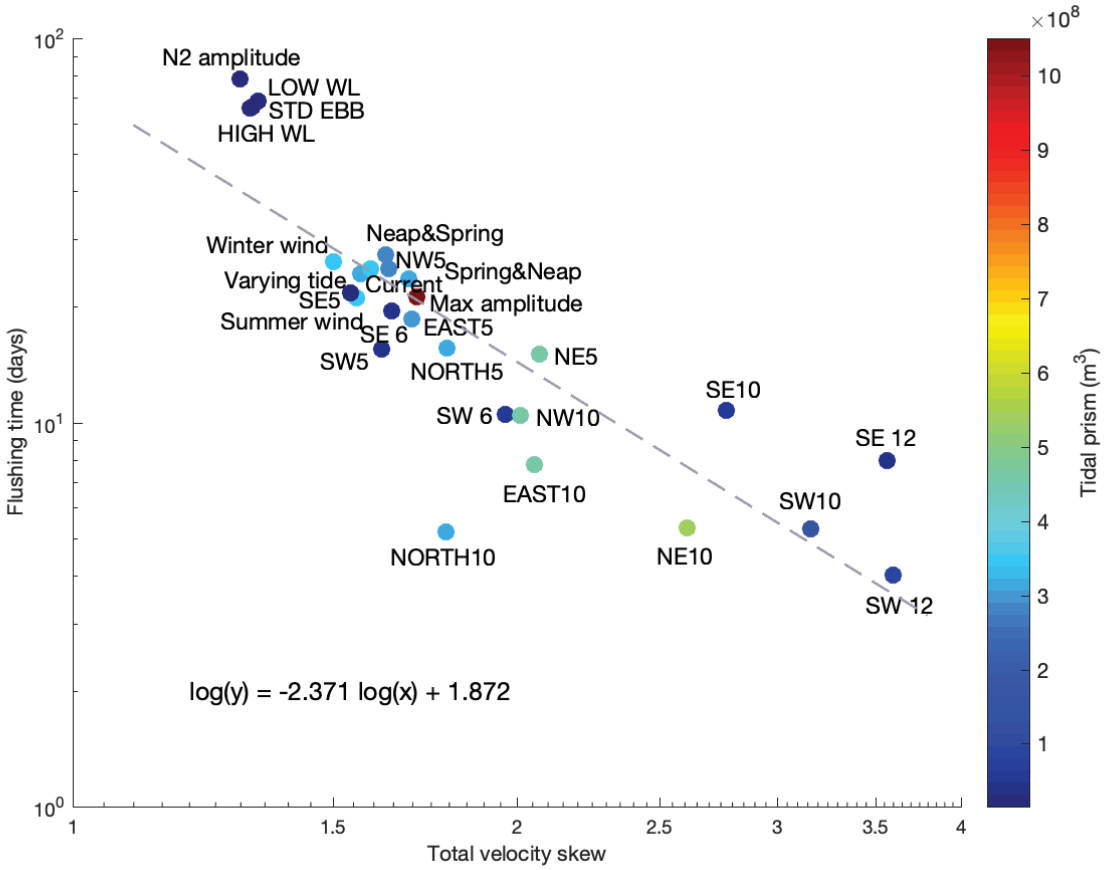

Figure 10. Flushing time of tracer as a function of tidal prism and total velocity skew. The grey line is the linear interpolation of the flushing time as a function of the total velocity skew. The equation of the linear model is indicated in the left bottom corner. Both *x* and *y* axes are in logarithmic scale.

[

535 4.3 One-dimensional model for computing flushing time under different wind conditions

536 Previous results refer to the most frequent conditions in terms of wind speed and direction.
537 However, since wind appears to be an effective forcing for flushing, additional simulations were
538 carried out for increments of wind speed of 5 m/s and every 45 degrees of wind direction (Table
539 4).
540
541 **Table 4.** Values of the coefficients of the single exponential function, flushing time, and R^2 and
542 *RSS* of the interpolation for the simulations including wind (simulations used for the polynomial
543 fit).
544

Simulation ID	**K**	**λ (days^{-1})**	**Flushing time (days)**	***Adjusted R^2***	***RSS***	***Variance of residuals***
No Wind	0.92330	0.03421	29.23	0.9795	0.1975	1.0000e-03
N5	1.02000	0.06403	15.62	0.9990	0.0102	5.8072e-05
N10	1.03200	0.19320	5.18	0.9980	0.0104	4.7768e-05
NE5	1.01700	0.06653	15.03	0.9991	0.0092	4.9934e-05
NE10	1.02400	0.18840	5.31	0.9990	0.0054	2.4527e-05
E5	1.00400	0.05378	18.59	0.9992	0.0085	4.5660e-05
E10	1.01600	0.12890	7.76	0.9993	0.0048	2.6462e-05
SE5	0.98530	0.04592	21.78	0.9985	0.0166	8.8675e-05
SE10	1.02700	0.09284	10.77	0.9994	0.0054	3.0003e-05
S5	1.02200	0.06421	15.58	0.9990	0.0112	6.1717e-05
S10	1.03900	0.18190	5.50	0.9983	0.0093	4.3930e-05
SW5	1.01400	0.06447	15.51	0.9990	0.0103	5.5191e-05
SW10	1.04400	0.18940	5.28	0.9984	0.0086	4.3941e-05
W5	1.00900	0.05372	18.61	0.9989	0.0123	6.5706e-05
W10	1.02000	0.11910	8.39	0.9995	0.0039	2.1251e-05
NW5	0.97810	0.04234	23.62	0.9974	0.0286	1.4887e-04
NW10	1.05000	0.09581	10.44	0.9985	0.0141	7.7408e-05

545

For each simulation, the mass fraction of the tracer inside the lagoons is fitted using a single exponential decay, as in the previous simulations including wind (Table 3). The decrease of mass fraction inside the lagoons becomes more rapid as the wind speed increases (Figure 11), with the fastest decay reached when the velocity is equal to 10 m/s and the wind is blowing in the direction parallel to the coast (northeast and southwest). Conversely, when the wind blows perpendicular to the barrier islands (northwest and southeast), it facilitates the reintroduction of the tracer that has left the lagoons through the inlets. The mass fraction decay triggered by winds from southwest and northeast presents an analogous exponential trend. Similarly, winds blowing from southeast and northwest yield a similar flushing time.

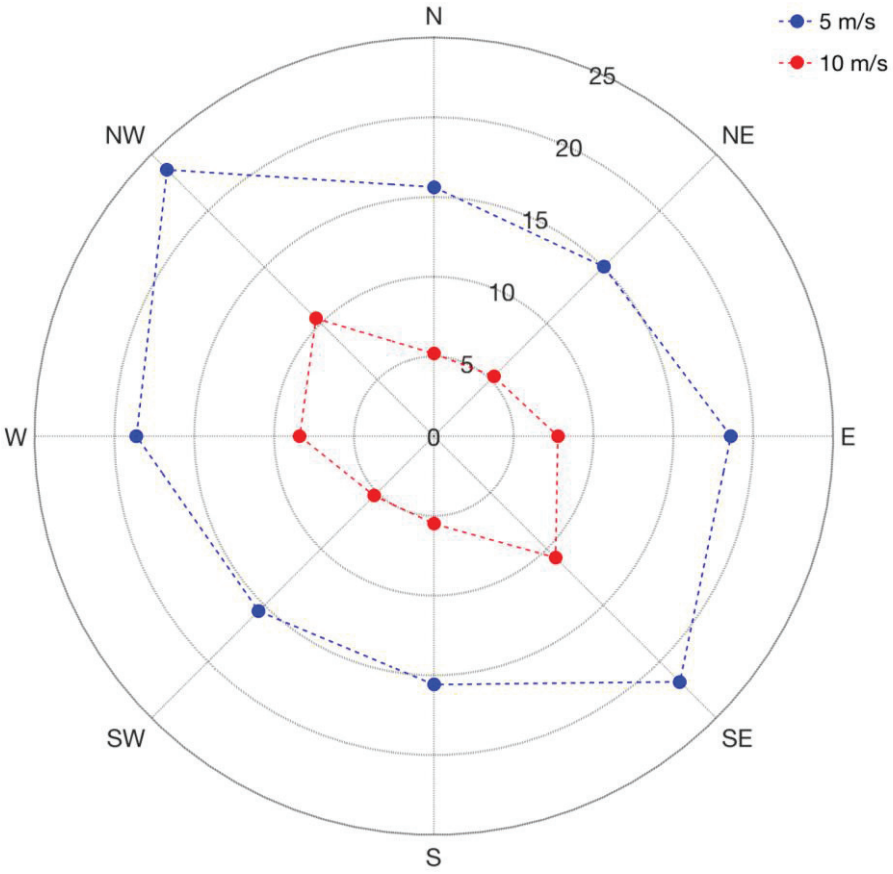

Figure 11. Flushing time distribution (days) as a function of the wind speed (in blue and red) and direction for the simulations with constant wind.

[

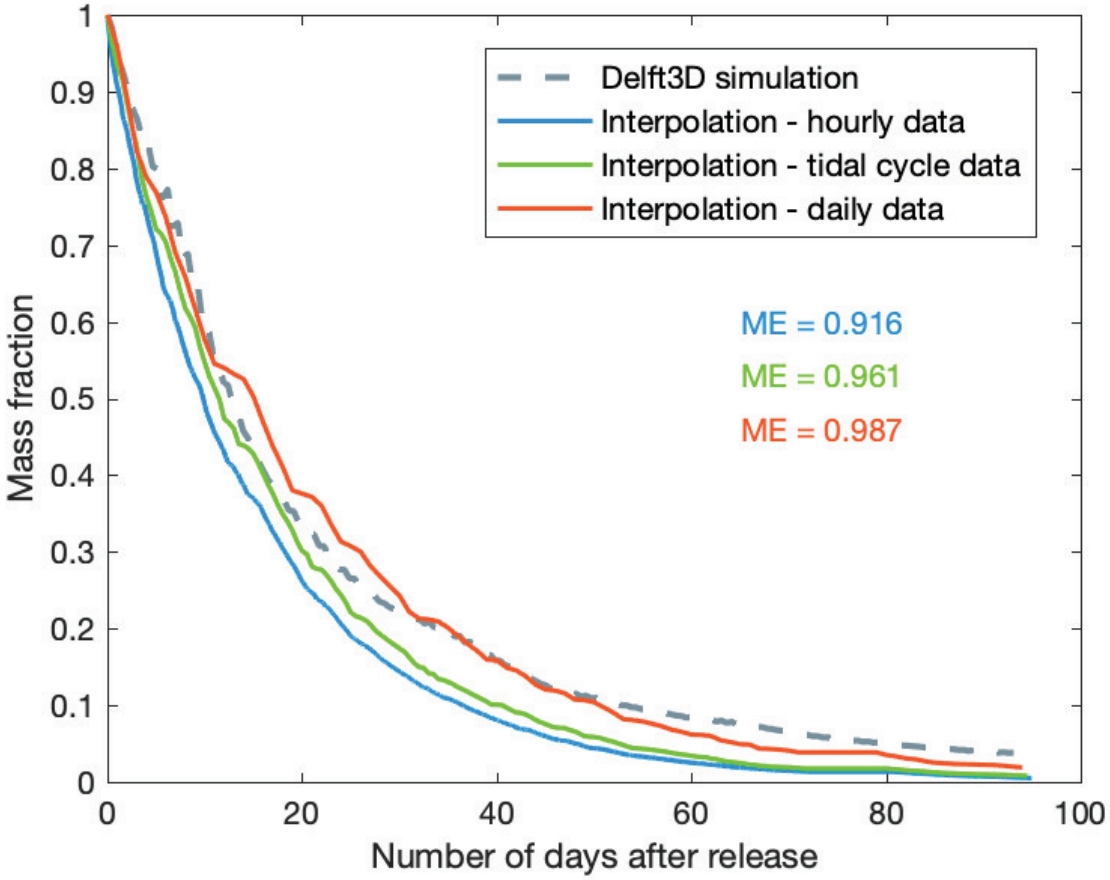

Figure 12. Comparison between the mass fraction decay derived from the Delft3D simulation and the mass fraction decay derived from the application of the polynomial function to the hourly, tidally and daily averaged wind data in the summer season of 2015.

The analytical method based on Equations 7 and 8 successfully reproduces the general mass decay behavior simulated by Delft3D (Figure 12). It is observed that the mass fraction retained in the system at the end of the simulation is better reproduced by the interpolation made with the daily averaged wind data, while tidally averaged, and hourly wind data are found to better interpolate the decay in the first days. The decay function varies depending on the interval over which the wind is averaged (one hour, one tide, one day) because the interpolating polynomial function is not linear.

[

572 **5 Discussion**

573 In the scenarios with Neap and Spring tides and without wind (Table 2, *SPRING&NEAP* and
574 *NEAP&SPRING*) the Eulerian approach adopted in this analysis produced a higher flushing time
575 than the values obtained with the Lagrangian method in Safak et al. [2015]: from 10 to almost 28
576 days in the case of the bays closer to the inlet. The reason for this is that the approach followed
577 by Safak et al. [2015] does not consider that a significant amount of particles that leave the
578 system during ebb can reenter the bays during flood, resulting in an underestimation of the actual
579 flushing time. On the other hand, coastal processes might facilitate the removal of the tracer once
580 it reaches the nearshore area outside the inlets, and thus, determine a faster decay of the tracer
581 mass. Here some of these processes, such as waves and wave-driven longshore currents, are not
582 included in the simulations and this might cause a change in flushing time. There is a difference
583 of approximately two days between the flushing time observed after the tracer is released during
584 high and low water levels, and this result seems to be in accordance with the median flushing
585 time evaluated in Safak et al. [2015] for almost all the bays having a direct connection to an inlet.
586 Also, the decrease in flushing time when wind is included in the model is in agreement with
587 Safak et al. [2015], and the magnitude of the decrease is a function of the velocity and direction
588 of the simulated wind. Specifically, the flushing time was lower during the summer of 2015
589 because a storm brought strong winds from northeast, a wind scenario that favors flushing
590 (Figure 11).

591 The particle tracking approach adopted by Safak et al. [2015] allows the evaluation of the
592 spatial distribution of the flushing time at each location, and shows that the parts of the bays
593 located near the inlets are more sensitive to tidal phase than wind forcing [Safak et al., 2015;
594 Fugate et al., 2006]. Here the Eulerian method provides a single value that defines the overall
595 flushing time of the tracer for all bays, regardless of the point of release. The entire system of
596 lagoons is more sensitive to wind forcing and differences in tidal phase along the coast than to
597 instant of release, indicating that the global flushing time is more affected by the flushing time
598 associated with the bays found in the interior region of the domain rather than in the areas
599 located near the inlets.

600 Defne and Ganju [2014] analyzed the influence of tides, coastal, riverine, and meteorological
601 processes on flushing time. They found that the percentage of particles removed from the domain
602 increases with the progressive addition of forcings to the scenario with only tides. However, in

603 that study the effects of each single factor were not investigated, and it is difficult to determine
604 what mechanism caused the greatest reduction in flushing time. Defne and Ganju [2014]
605 concluded that remote coastal forcings (i.e., tidally averaged water levels and currents added to
606 the tidal oscillations at the open boundaries) and meteorological forcings (surface air pressure,
607 wind speed and direction) were the most effective in the removal of particles.
608 In the scenarios of this study including the meteorological forcing, i.e. wind conditions, it has
609 been observed that as wind speed increases the mass decay occurs at a faster rate, and therefore
610 the flushing time of the tracer decreases. This is because wind-driven circulation produces
611 asymmetric fluxes of water between the lagoon and the ocean. Note that our synthetic scenarios
612 assume a wind speed that is constant in intensity and direction for an unrealistic long time, so the
613 resulting mass decay should be seen as a theoretical value. On the other hand, in our proposed
614 simplified model (Equation 7 and 8) the decay rate is changed every few hours to account for
615 wind variability in a realistic manner.
616 Given the highest wind speed (12 m/s), the most effective wind direction in the removal of
617 tracer particles is observed to be the southwest direction, corresponding to the direction parallel
618 to the inlets of the lagoons. In this scenario the tracer leaving the lagoons is not able to re-enter
619 into the system because the wind-generated currents are moving northwest. Moreover, the
620 Ekman transport facilitates the exchange of water and particles when the wind blows parallel to
621 the coast, increasing storm surges and extreme low tides [Fagherazzi et al., 2010]. Fagherazzi et
622 al. [2010] indicate that Ekman transport can increase the water level in the VCR lagoons by 0.2-
623 0.4 m, which roughly corresponds to an increase in tidal prism between 15% and 30%, and
624 therefore an increase of the fluxes in and out the system. These fluxes also vary across the inlets,
625 producing velocity asymmetry in flood and ebb and tracer dispersion (Figure 10).
626 On the other hand, in the scenario with a wind direction blowing landwards perpendicular to
627 the coastline (southeast direction), the particles exit and re-enter the system several times through
628 the inlets, producing a slower decay of the tracer concentration inside the lagoons. In addition,
629 the tracer that remains in the lagoons is pushed toward the northern bays of VCR, where the
630 inlets are smaller, and thus, the exchange of the tracer particles between the bays and the open
631 ocean takes place at a lower rate.
632 A wind perpendicular to the barrier islands but blowing from land towards ocean (northwest
633 direction) increases at first the flushing of the tracer by producing a setdown and a large outward

discharge. However, for continuity, a sizable water flux will also occur during the next flood phase to replenish the lagoons with the water lost during the setdown. This phenomenon was also observed by Fagherazzi and Priestas [2010] in the Louisiana coast. Wind blowing perpendicular to the coast increased the flux of sediment toward the ocean at first, but then the sediment re-entered the system during the following tidal cycle. The overall effect of a wind perpendicular to the shore is an increase in water fluxes in and out of the system and a slight velocity skew in the inlets, moderately increasing the flushing of the tracer.

A wind parallel to the shore produces instead a strong asymmetry in circulation, with flow exiting the bays from one inlet and re-entering from a different one so that most of the tracer exiting the system does not return (Figure 9). Field measurements and numerical simulations carried out by Li [2013] in a bay with three inlets and wind blowing parallel to the shore indicate that a net outward flow takes place at the downwind inlet, while a net inward flow occurs at the inlet located upwind. As a result, fluxes during ebb are not rebalanced by symmetric fluxes during flood within the same inlet, dramatically increasing the overall tracer removal from within the lagoons.

When the variability in wind direction is accounted for, the flushing time becomes more similar to the simulations without wind (Table 3). This is because most of the time the wind is weak (Figure 3). We do notice a sharp decrease in flushing time with summer winds. While on average the measured winds were higher in winter, in the summer of 2015 a storm occurred that triggered winds above 10 m/s (Figure 3). The maximum wind blew from northeast, along the shallow bays, which we showed being one of the directions more favorable for tracer flushing (Table 4). Of all the simulations with realistic tidal and wind conditions, the one with summer winds led to the lowest flushing time (21.07 days). We therefore conclude that winds do exert control on the flushing of the system, but only if they blow along the bays and not perpendicularly to them. Moreover, infrequent events with high wind speed are more important than average wind conditions.

We conclude that processes triggering asymmetric fluxes between the bays and the ocean, such as wind-driven subtidal circulation, and differences in tidal phase and amplitude along the shore are the most successful at flushing tracer. Processes that augment the fluxes of water in and out the bays, such as wind driven storm surges and setup caused by Ekman transport, also enhance tracer flushing, but to a lower degree and partly through an increase in velocity skew.

Some of these results might be only valid for coastal bays with multiple inlets. In fact, if only one inlet is present, subtidal circulation driven by wind is likely absent, since all the water is entering and exiting from the same inlet. Wind can still trigger surges and Ekman transport, thus increasing the volume of water exchanged with the ocean and therefore flushing, but the lack of asymmetric flows will increase the overall flushing time of the tracer.

In this study we have not considered wind generated waves and long-shore currents. Based on our findings, it seems likely that wave-driven long-shore currents would favor the dispersion of tracer by creating asymmetric fluxes at the inlets, similarly to what wind-driven currents do. More research is needed to determine the role of wave-breaking and long-shore currents on tracer dispersion.

6 Conclusions

Semi-enclosed water bodies, such as bays and lagoons, host ecosystems sensitive to the release of nutrients and pollutants due to human activities along the coast. Therefore, understanding the decay and flushing time of tracers has important environmental consequences. Given a system of bays, the mean flushing time associated to the entire area can be evaluated by using hydrodynamic models and an Eulerian based approach. In this paper, the transport of a tracer within the system of shallow bays in the VCR has been simulated using the hydrodynamic model Deflt3D. The decrease in time of the tracer mass follows an exponential decay function. Specifically, a double exponential function was found to better approximate the tracer decay when the effect of wind is neglected, while a single exponential function is a good approximation when the wind effect is included in the simulations. We further identified factors producing the shortest flushing time of the tracer within a system with multiple inlets. We show that asymmetry in ebb-flood velocity at the inlets is responsible for the rapid decay of the tracer mass in the lagoons. These asymmetries, computed with a velocity skew index, are generated by differences in tidal phase and amplitude along the inner shelf and by wind-driven circulation under non-storm conditions.

In general, the average flushing time of the VCR bays is around 25-27 days. When the difference in tidal phase along the Atlantic coast is accounted for, the flushing time decreases to 24 days, due to asymmetric tidal fluxes at the inlets. Winds can also decrease the flushing time, but only if they are strong and blow along the bays (from southwest or northeast). In the summer

of 2015, strong winds reduced the flushing time to 21 days. Currents triggered by shelf circulation do not seem to affect the flushing of the system.

A simple exponential decay function using wind-dependent parameters calculated with a polynomial regression (Equation 7 and 8) can be used to estimate the decay in concentration without the need of a hydrodynamic model. This function well predicted the tracer mass decrease during the summer months of 2015 in the VCR bays. This result demonstrates that the average flushing time of tracer within the entire system of bays in the Virginia Coast Reserve can be estimated from the evaluation of a single parameter, which controls the exponential decay of the tracer mass inside the lagoons.

Acknowledgments, Samples, and Data

This research was supported by NSF Awards 1832221 (VCR-LTER Program), and 1637630 (PIE-LTER Program).

References

Abbott M.B., and Cunge J.A., (1975). Two-dimensional modelling of tidal deltas and estuaries, case study: River Seine Estuary Coarse Grid Model, In: Unsteady Flows in Open Channels, Series, Mahmood K and Yevhevich V (eds), 795-799, Water Res. Publications.

Aikman F., III, and L.W.J. Lanerolle (2004), Report on the National Ocean Service Workshop on Residence/Flushing Times in Bays and Estuaries. *NOAA Office of Coastal Survey, Silver Spring, MD.* Available online at: http://www.nauticalcharts.noaa.gov/csdl/publications/TR_NOS-CS20_FY05_Aikman_ResidenceTimeWorkshopReport.pdf.

Allen T.R., Oertel G.F., McLeod G. (2011), Synoptic assessment of repletion and residual water dynamics in a coastal lagoon by thermal remote sensing: great Machipongo Lagoon (Hog Island Bay), Virginia, USA. IEEE *Journal of Selected Topics in Applied Earth Observations and Remote Sensing*, 4(1), 147-158.

Anderson, I., Stanhope J., McGlathery K., Overman K., 2009. Discharge of three small creeks along the Delmarva Peninsula 2003-2009. *Virginia Coast Reserve Long-Term Ecological*

Research Project Data Publication, knb-lter-vcr.160.19, doi:doi:10.6073/pasta/e4cb2542a256511e5e91e17a674a4c01.

Andutta F. P., Ridd P. V., Wolanski E., 2012. The age and the flushing time of the Great Barrier Reef waters. *Continental Shelf Research*, 53, 11-19.

Braunschweig F., Martins F., Chambel P., Neves R. (2003), A methodology to estimate renewal time scales in estuaries: the Tagus Estuary case. *Ocean Dynamics*, 53, 137-145.

Burwell D., Vincent M., Luther M., Galperin B. (2000), In: Spaulding, M.L., Butler, H.L. (Eds.), Estuarine and Coastal Modeling. *American Society of Civil Engineers*, Reston, VA, 995–1009.

Cavalcante G.H., Kjerfve B., Feary D.A. (2012), Examination of residence time and its relevance to water quality within a coastal mega-structure: The Palm Jumeirah Lagoon. *Journal of Hydrology*, 468-469, 111-119.

Choi K.W. and Lee J.H.W. (2004), Numerical determination of flushing time for stratified water bodies. *Journal of Marine Systems*, 50, 263-281.

Cucco, A., Umgiesser, G., Ferrarin, C., Perilli, A., Canu, D.M. and Solidoro, C. (2009), Eulerian and lagrangian transport time scales of a tidal active coastal basin. *Ecological Modelling*, 220(7), 913-922.

Cunge J.A. (2003). Of data and models. *Journal of Hydroinformatics*, 5 (2), 75-98.

Defne Z. and Ganju N.K. (2014), Quantifying the residence time and flushing characteristics of a shallow, back-barrier estuary: application of hydrodynamic and particle tracking models. *Estuaries and Coasts*, DOI 10.1007/s12237-014-9885-3.

Delhez É.J.M. (2005), Transient residence and exposure times. *Ocean Science*, 2, 1-9.

Delhez É.J.M. and Deleersnijder É. (2006), The boundary layer of the residence time field. *Ocean Dynamics*, 56, 139-150.

Deleersnijder E., Campin J. M., Delhez É.J.M., 2001. The Concept of Age in Marine Modelling. I. Theory and Preliminary Model Results. *Journal of Marine Systems*, 28(3), 229-267, doi: 10.1016/S0924-7963(01)00026-4.

Du J., Park K., Shen J., Dzwonkowski B., Yu X., Yoon B. I., 2018. Role of baroclinic processes on flushing characteristics in a highly stratified estuarine system, Mobile Bay, Alabama. *Journal of Geophysical Research: Oceans*, 123, 4518–4537, doi: 10.1029/2018JC013855.

Dyer, K. R. (1973). *Estuaries: A physical introduction*, Wiley, New York.

[

754 Fagherazzi S., Mariotti G., Porter J. H., McGlathery K. J., and Wiberg P. L. (2010), Wave energy
755 asymmetry in shallow bays. *Geophysical Research Letters*, 37, L24601,
756 doi:10.1029/2010GL045254.
757 Fagherazzi S. and Wiberg P.L. (2009) Importance of wind consitions, fetch, and water levels on
758 wave-generated shear stresses in shallow intertidal basins. *Journal of Geophysical*
759 *Research*, 114, F03022, doi:10.1029/2008JF001139.
760 Fagherazzi, S. and Priestas, A.M., (2010). Sediments and water fluxes in a muddy coastline:
761 interplay between waves and tidal channel hydrodynamics. *Earth Surface Processes and*
762 *Landforms*, 35(3), pp.284-293.
763 Fugate D.C., Friedrichs C.T., Bilgili A. (2006), Estimation of residence time in a shallow back
764 barrier lagoon, Hog Island Bay, Virginia, USA. *Estuarine and Coastal Modeling 2005*,
765 319-337.
766 Guo, Q. and Lordi G. P. (2000), Method for quantifying freshwater input and flushing time in
767 estuaries. *Journal of Environmental Engineering*, 126, 675-683.
768 Herrling, G. and Winter, C., (2015). Tidally-and wind-driven residual circulation at the multiple-
769 inlet system East Frisian Wadden Sea. *Continental Shelf Research*, 106, 45-59.
770 Lentz, S.J., 2008. Observations and a model of the mean circulation over the Middle Atlantic Bight
771 continental shelf. *Journal of Physical Oceanography*, *38*(6), 1203-1221.
772 Lesser, G.R., Roelvink, J.A., Van Kester, J.A.T.M. and Stelling, G.S. (2004), Development and
773 validation of a three-dimensional morphological model. *Coastal engineering*, 51(8), 883-
774 915.
775 Leonardi, N., Canestrelli, A., Sun, T. and Fagherazzi, S. (2013), Effect of tides on mouth bar
776 morphology and hydrodynamics. *Journal of Geophysical Research: Oceans*, 118(9),
777 4169-4183.
778 Leonardi, N., Kolker, A.S. and Fagherazzi, S. (2015), Interplay between river discharge and tides
779 in a delta distributary. *Advances in Water Resources*, *80*, 69-78.
780 Li, C., (2013). Subtidal water flux through a multiple-inlet system: Observations before and during
781 a cold front event and numerical experiments. *Journal of Geophysical Research:*
782 *Oceans*, 118(4), pp.1877-1892.

783 Mariotti G., Fagherazzi S., Wiberg P. L., McGlathery K. J., Carniello L., Defina A. (2010),
784 Influence of storm surges and sea level on shallow tidal basin erosive processes. *Journal*
785 *of Geophysical Research*, 115, C11012, doi:10.1029/2009JC005892.
786 McGlathery K., Christian R., 2018. Water Quality Sampling - integrated measurements for the
787 Virginia Coast, 1992-2018. *Virginia Coast Reserve Long-Term Ecological Research*
788 *Project Data Publication*, knb-lter-vcr.247.10,
789 doi:doi:10.6073/pasta/b650b236f092e0fdee0d5d8ccf521cb3.
790 Monsen N. E., Cloern J. E., Lucas L., Monismith S. G. (2002), A comment on the use of flushing
791 time, residence time, and age as transport time scales. *Limnology and*
792 *Oceanography*, 47(5), 1545-1553, doi: 10.4319/lo.2002.47.5.1545.
793 Mukai, A.Y., Westerink, J.J., Luettich Jr, R.A. and Mark, D., (2002). Eastcoast 2001, a tidal
794 constituent database for western North Atlantic, Gulf of Mexico, and Caribbean Sea (No.
795 ERDC/CHL-TR-02-24). *Engineer Research and Development Center Vicksburg Ms*
796 *Coastal and Hydraulicslab*.
797 Nardin W., Larsen L., Fagyherazzi S., Wiberg P., 2018. Tradeoffs among hydrodynamics,
798 sediment fluxes and vegetation community in the Virginia Coast Reserve, USA.
799 *Estuarine, Coastal and Shelf Science*, 210, 98-108.
800 Nidzieko, N.J. and Ralston, D.K. (2012). Tidal asymmetry and velocity skew over tidal flats and
801 shallow channels within a macrotidal river delta. *Journal of Geophysical Research:*
802 *Oceans*, 117(C3).
803 Pawlowicz R., Beardsley B., Lentz S. (2002). Classical tidal harmonic analysis including error
804 estimates in MATLAB using T_TIDE, *Computers and Geosciences,* 28, 929-937.
805 Patgaonkar R.S., Vethamony P., Lokesh K.S., Babu M.T. (2012), Residence tie of pollutants
806 discharged in the Gulf of Kachchh, northwestern Arabian Sea. *Marine Pollution Bulletin*,
807 64(8), 1659-1666.
808 Periáñez R., Casas-Ruíz M., Bolívar J.P. (2013), Tidal circulation, sediment and pollutant transport
809 in Cádiz Bay (SW Spain): A modelling study. *Ocean Engineering*, 69, 60-69.
810 Rayson M. D., Gross E. S., Hetland R. D., Fringer O. B., 2016. Time scales in Galveston Bay: An
811 unsteady estuary. *Journal of Geophysical Research: Oceans*, 121, 2268–2285,
812 doi:10.1002/2015JC011181.

Roelvink D.J.A. and Van Banning G.K.F.M. (1994), Design and development of Delft3D and application to coastal morphodynamics. *Hydroinformatics*, 94, 451-455.

Safak I., Wiberg P.L., Richardson D.L., Kurum M.O. (2015), Controls on residence time and exchange in a system of shallow coastal bays. *Continental Shelf Research*, 97, 7-20.

Scully M.E., 2013. Physical controls on hypoxia in Chesapeake Bay: A numerical modeling study. *Journal of Geophysical Research: Oceans*, *118*(3), 1239-1256.

Szpilka C., Dresback K., Kolar R., Feyen J., Wang J. (2016). Improvements for the western north atlantic, caribbean and gulf of mexico adcirc tidal database (EC2015). *Journal of Marine Science and Engineering*, 4(4), 72.

Takeoka H., 1984. Fundamental concepts of exchange and transport time scales in a coastal sea. *Continental Shelf Research*, 3, 311-326.

Wiberg P.L., Carr J.A., Safak I., Anutaliya A. (2015), Quantifying the distribution and influence of non-uniform bed properties in shallow coastal bays. *Limnology and Oceanography: Methods*, 13, 746-762.

Williams L. (1986), Flushing time calculations for the Upper Waitemata Harbour, New Zealand. *New Zealand Journal of Marine and Freshwater Research*, 20:3, 455-465, doi:10.1080/00288330.1986.9516165.

Continental Shelf Research Journal

Supporting Information for

Velocity skew controls the flushing of a tracer in a system of shallow bays with multiple inlets

I. Palazzoli[1,2], N. Leonardi[3], A. M. Jiménez-Robles[1,4], S. Fagherazzi[1]

[1]Department of Earth and Environment, Boston University, Boston, MA, USA.
[2]Department of Civil, Chemical, Environmental and Materials Engineering, University of Bologna, Italy.
[3]Department of Geography and Planning, University of Liverpool, Liverpool, UK.
[4]Environmental Fluid Dynamics Group, Andalusian Institute for Earth System Research, University of Granada, Granada, Spain.

Contents of this file

Tables S1 and S2, Figure S1 to S3.

Introduction

This supporting information provides data that were used to set up the simulations in the Delft3D-FLOW model and results that were obtained from the simulations in the Delft3D-FLOW model. Specifically, Table S1 shows the values of the amplitude and phase of the tidal harmonics observed at Wachapreague station before and after the calibration. These data were employed to reproduce the water level at the open boundaries of the domain. The manual calibration was done by comparing the water level observed at Wachapreague station and the water level reproduced by the model at the same location. Table S2 compares the coefficient of correlation, R^2, the error sum of squares, *RSS*, and the variance of residuals for the interpolation of the decay of the tracer mass fraction using a single and a double exponential function.

Figure S1 shows the difference in amplitude and phase between the main harmonic constituents measured by NOAA at the Wachapreague station and the harmonic constituents simulated by Delft3D with the ADCIRC boundary conditions at the Wachapreague location. Figure S2 shows the difference between single and double exponential fit for the STD EBB scenario. Finally, Figure S3 shows the residual velocity in the main inlets of VCR obtained from the *VARYING TIDE* simulation.

Table S1. Amplitude and phase of the harmonic constituents before and after the calibration carried out at Wachapreague station.

			Observed values		Calibrated values	
Constituent #	**Name**	**Description**	**Amplitude [m]**	**Phase [deg]**	**Amplitude [m]**	**Phase [deg]**
1	M2	Principal lunar semidiurnal constituent	0.48675	241.8	0.486750	241.8
2	S2	Principal solar semidiurnal constituent	0.08415	273.2	0.084150	273.2
3	N2	Larger lunar elliptic semidiurnal constituent	0.10395	234.7	0.103950	234.7
4	K1	Lunar diurnal constituent	0.06930	128.7	0.069300	128.7
5	M4	Shallow water overtides of principal lunar constituent	0.02500	291.9	0.020625	291.9
6	O1	Lunar diurnal constituent	0.08700	146.9	0.071775	146.9

Table S2. Values of the adjusted coefficient of determination, R^2, the residual sum of squares, *RSS,* and the variance of residuals of the double and single exponential function for each simulation with and without wind.

	Single exponential			**Double exponential**		
Simulation ID	***Adjusted R^2***	***RSS***	***Variance of residuals***	***Adjusted R^2***	***RSS***	***Variance of residuals***
STD EBB	0.9963	0.0429	1.7530e-04	0.9998	0.0026	1.0450e-05
STD FLOOD	0.9953	0.0623	2.4832e-04	0.9997	0.0033	1.3377e-05
HIGH WL	0.9960	0.0459	1.8768e-04	0.9997	0.0039	1.6015e-05
LOW WL	0.9968	0.0400	1.6256e-04	0.9999	6.1386 e-04	2.4955e-06
MAX AMPLITUDE	0.9554	0.3703	0.0013	0.9987	0.0111	4.5982e-05
N2 AMPLITUDE	0.9970	0.0318	1.3068e-04	0.9999	0.0013	5.1807e-06
SPRING&NEAP	0.9666	0.3742	0.0014	0.9929	0.0793	3.3051e-04
NEAP&SPRING	0.9684	0.3069	0.0012	0.9976	0.0231	9.8742e-05
VARYING TIDE	0.9764	0.2439	8.5070e-04	0.9993	0.0067	2.8694e-05
CURRENT	0.9759	0.2512	8.9710e-04	0.9991	0.0094	4.0337e-05
SE6	0.9990	0.0136	4.7807e-05	0.9988	0.0165	5.5712e-05
SE12	0.9995	0.0420	1.1907e-04	0.9993	0.0059	2.4291e-05
SW6	0.9972	0.0278	8.4867e-05	0 .9975	0.0250	1.0514e-04
SW12	0.9921	0.0392	1.3950e-04	0.9968	0.0155	6.5896e-05
WINTER WIND	0.9632	0.2266	0.0012	0.9947	0.0322	1.8824e-04
SUMMER WIND	0.9874	0.1295	6.1193e-04	0.9970	0.0306	1.6880e-04

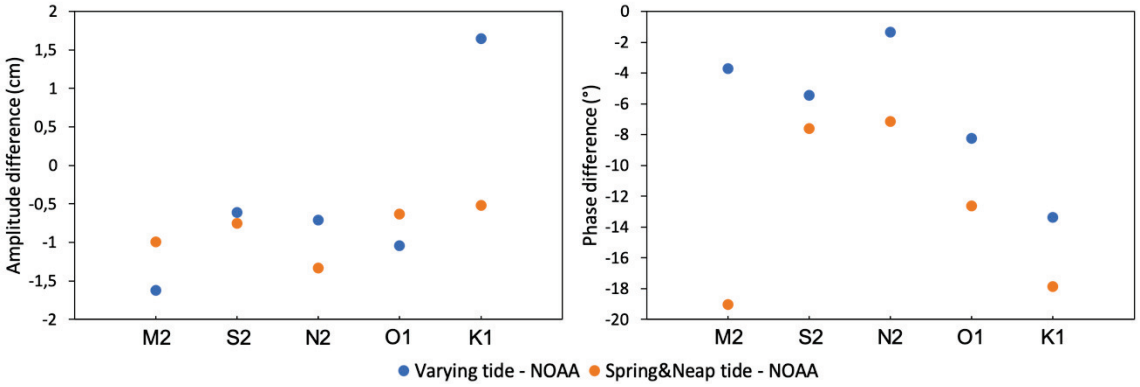

Figure S1. Difference between the amplitude and phase of M2, S2, N2, O1, and K1 harmonics observed at NOAA Wachapreague station and derived from Delft3D simulations of the *VARYING TIDE* and *SPRING&NEAP* tide scenarios.

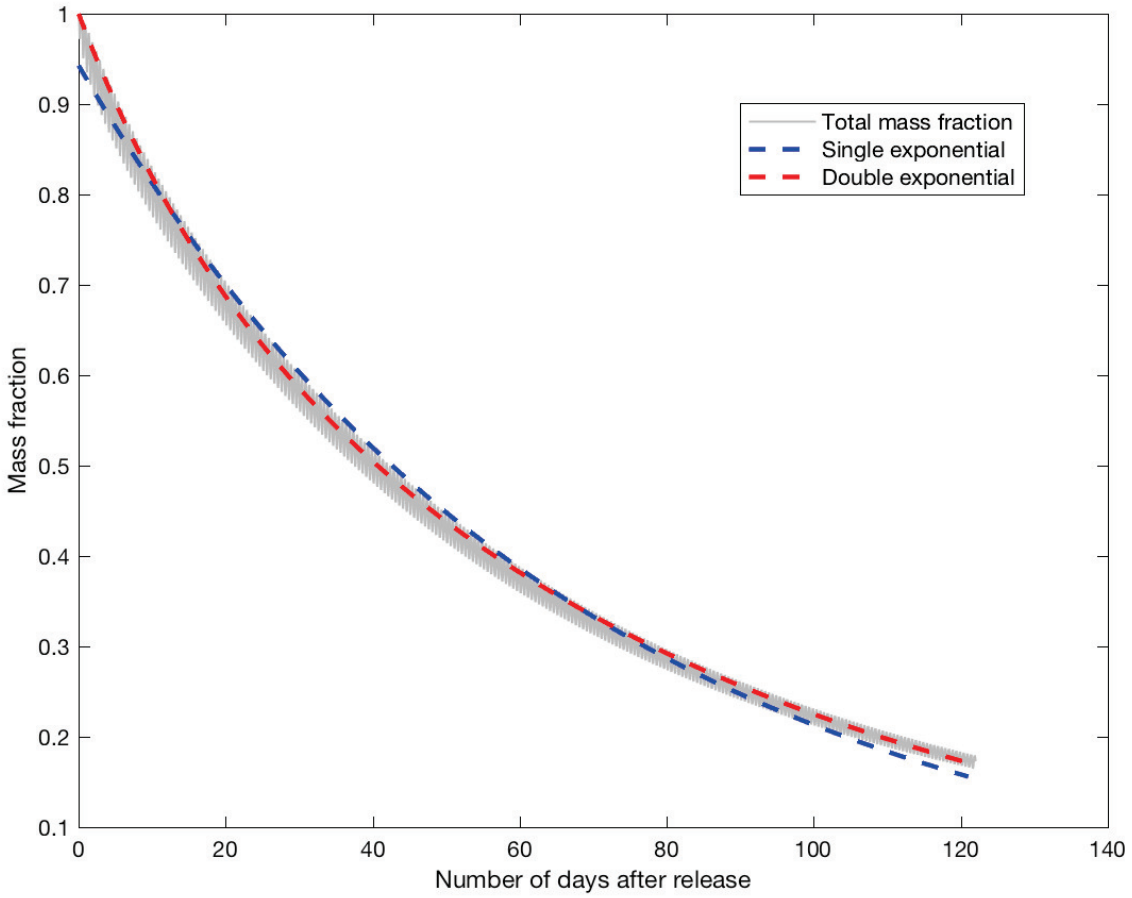

Figure S2. Comparison between single and double exponential fit for the *STD EBB* simulation (standard conditions, ebb starting point). The grey line represents the decaying mass fraction calculated as integral over the entire bay. The blue dashed line represents the single exponential fit to the mass fraction decay, as in Equation 3, whereas the red dashed line is the double exponential fit of Equation 1. Adjusted R^2, RSS and Variance of residuals can be found in Table S2 of the Supporting Information.

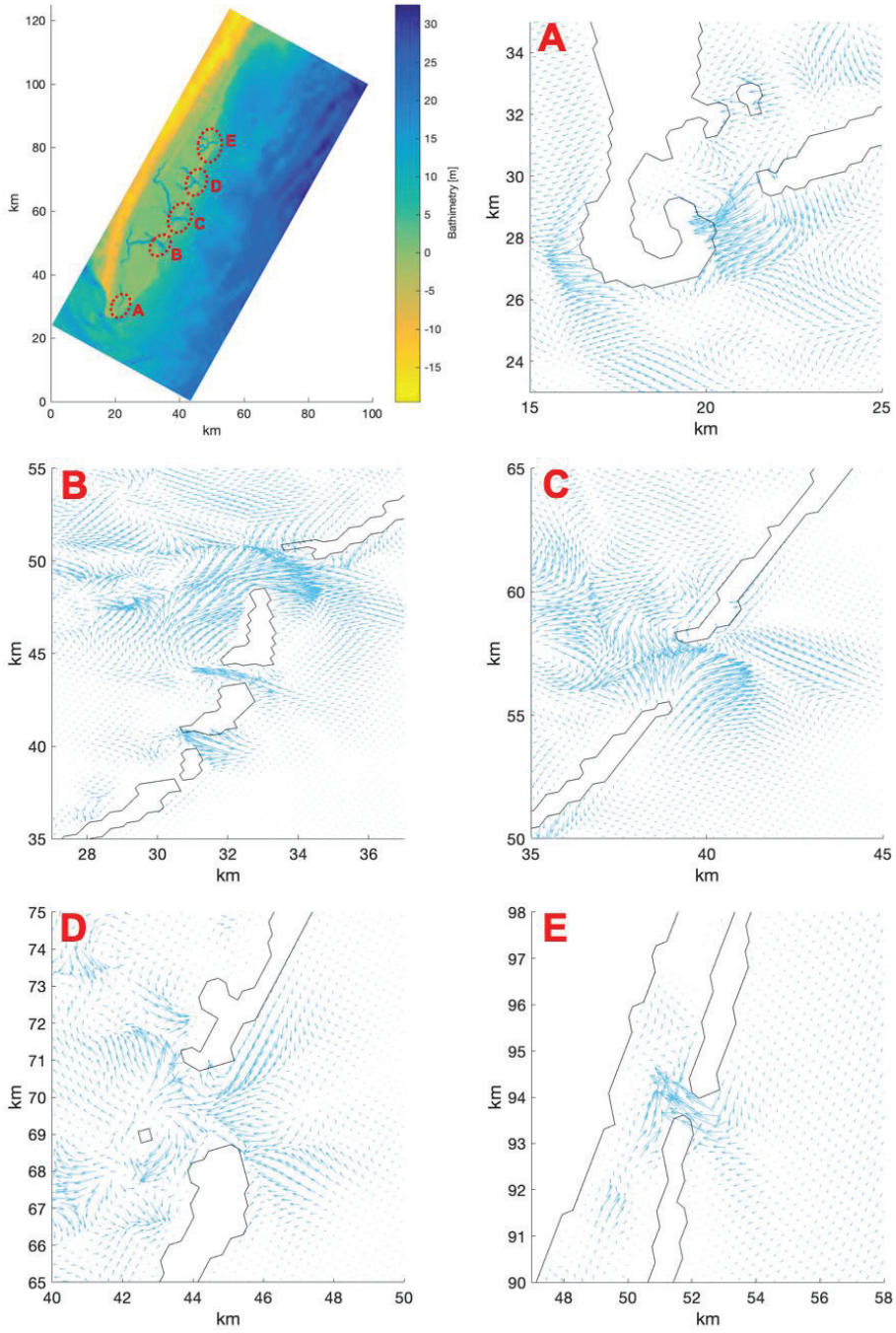

Figure S3. Residual velocity in the main inlets of VCR obtained from the *VARYING TIDE* simulation.

Conflict of Interest Statement

Manuscript title: *Velocity skew controls the flushing of a tracer in a system of shallow bays with multiple inlets*

The authors declare that they have no known competing financial interests or personal relationships that could have appeared to influence the work reported in this paper.

Bologna, 10/09/2019

Irene Palazzoli